

1 **Distinguishing the drivers of trends in land carbon fluxes and plant volatile**
2 **emissions over the past three decades**

3
4 X. Yue ¹, N. Unger ¹, Y. Zheng ²

5
6 ¹ School of Forestry and Environment Studies, Yale University, New Haven, Connecticut
7 06511, USA

8 ² Department of Geology and Geophysics, Yale University, New Haven, Connecticut
9 06511, USA

10
11
12
13
14
15

Correspondence to: X. Yue (xuyueseas@gmail.com)

Abstract

The terrestrial biosphere has experienced dramatic changes in recent decades. Estimates of historical trends in land carbon fluxes remain uncertain because long-term observations are limited on the global scale. Here, we use the Yale Interactive terrestrial Biosphere (YIBs) model to estimate decadal trends in land carbon fluxes and emissions of biogenic volatile organic compounds (BVOCs) and to identify the key drivers for these changes during 1982-2011. Driven with hourly meteorology from WFDEI (WATCH Forcing Data methodology applied to ERA-Interim data), the model simulates an increasing trend of 297 Tg C a^{-2} in gross primary productivity (GPP) and 185 Tg C a^{-2} in the net primary productivity (NPP). CO_2 fertilization is the main driver for the flux changes in forest ecosystems, while meteorology dominates the changes in grasslands and shrublands. Warming boosts summer GPP and NPP at high latitudes, while drought dampens carbon uptake in tropical regions. North of 30°N , increasing temperatures induce a substantial extension of 0.22 day a^{-1} for the growing season; however, this phenological change alone does not promote regional carbon uptake and BVOC emissions. Nevertheless, increases of LAI at peak season accounts for $\sim 25\%$ of the trends in GPP and isoprene emissions at the northern lands. The net land sink shows statistically insignificant increases of only 3 Tg C a^{-2} globally because of simultaneous increases in soil respiration. Global BVOC emissions are calculated using two schemes. With the photosynthesis-dependent scheme, the model predicts increases of 0.4 Tg C a^{-2} in isoprene emissions, which are mainly attributed to warming trends because CO_2 fertilization and inhibition effects offset each other. Using the MEGAN (Model of Emissions of Gases and Aerosols from Nature) scheme, the YIBs model simulates global reductions of 1.1 Tg C a^{-2} in isoprene and 0.04 Tg C a^{-2} in monoterpene emissions in response to the CO_2 inhibition effects. Land use change shows limited impacts on global carbon fluxes and BVOC emissions, but there are regional contrasting impacts over Europe (afforestation) and China (deforestation).

45 **1 Introduction**

46

47 The terrestrial biosphere interacts with the atmosphere through photosynthesis and
48 biogenic volatile organic compound (BVOC) emissions. Annually, terrestrial ecosystems
49 assimilate ~120 petagrams of carbon (Pg C) from the atmosphere (Beer et al., 2010),
50 most of which reenters atmosphere through respiration and decomposition, resulting in a
51 net global land carbon sink of $2.6 \pm 0.7 \text{ Pg C a}^{-1}$ (Le Quere et al., 2009; Sitch et al.,
52 2015). Global BVOC emissions are estimated to be about 1 Pg C per year (Carslaw et al.,
53 2010). These emissions are important precursors of atmospheric oxidants and aerosols,
54 both of which affect surface air quality and exert additional regional and global chemical
55 climate forcings (Scott et al., 2014; Unger, 2014). Observations and simulations have
56 shown significant changes in terrestrial carbon assimilation and BVOC emissions in the
57 past 2-3 decades (Lathiere et al., 2006; Sarmiento et al., 2010; Sindelarova et al., 2014;
58 Sitch et al., 2015). Understanding drivers of these trends is important for the projections
59 of future carbon fluxes, water cycle, air quality, and climatic responses.

60

61 Trends in land carbon assimilation and BVOC emissions are related to the changes in
62 atmospheric CO₂, meteorology, and human land use land cover change perturbations.
63 Elevated CO₂ promotes plant photosynthesis (Ainsworth and Long, 2005) but can
64 directly inhibit isoprene productions (Arneth et al., 2007). Warming accelerates both
65 carbon uptake and BVOC emissions when temperature is not above the thermal optimum
66 (25-30 °C for photosynthesis and 35-40 °C for isoprene emission) for ecosystems that are
67 not water-stressed (Farquhar et al., 1980; Guenther et al., 1993; Piao et al., 2013).
68 Additional warming above thermal optimum may decrease photosynthesis but still
69 promote respiration, reducing net carbon uptake by plants (Liang et al., 2013). Increased
70 temperatures also indirectly influence carbon exchange and BVOC emissions through the
71 extension of growing season (Piao et al., 2007). Drought decreases gross primary
72 productivity (GPP) and net primary productivity (NPP) (Zhao and Running, 2010), but
73 may temporally enhance isoprene emissions (Monson et al., 2007). Land use change
74 affects the regional carbon budget and BVOC emissions through either additional

75 emissions or land cover changes due to deforestation, forest management, and
76 agricultural activities (Lathiere et al., 2006; Houghton, 2010).

77

78 Estimates of recent decadal global trends in the land carbon budget and BVOC emissions
79 are limited and uncertain due to the lack of observations. The earliest site-level
80 measurements of land carbon fluxes were set up in the 1990s (Wofsy et al., 1993). The
81 flux tower data sets provide long-term records of regional carbon exchange with high
82 precision but low spatial representation. In contrast, satellite products, such as GPP and
83 NPP retrievals from the Moderate Resolution Imaging Spectroradiometer (MODIS)
84 (Zhao et al., 2005) and isoprene emissions based on tropospheric formaldehyde columns
85 from the Global Ozone Monitoring Experiment (Palmer et al., 2006), improve the spatial
86 coverage but usually are available for only a relatively short time period (months to
87 several years) and suffer from systematic biases when compared with ground
88 measurements (e.g., Heinsch et al., 2006; Marais et al., 2012). Terrestrial biosphere
89 models, evaluated with both site-level and satellite-based observations, are useful tools to
90 estimate trends and attribute drivers of changes in land carbon fluxes and BVOC
91 emissions (e.g., Mao et al., 2013; Stavrakou et al., 2014; Sitch et al., 2015).

92

93 In this study, we use the Yale Interactive Terrestrial Biosphere Model (YIBs, Yue and
94 Unger, 2015) driven with long-term reanalysis meteorology to study the global trends of
95 land carbon fluxes and BVOC emissions over the past three decades. The YIBs model is
96 a process-based vegetation model that simulates complete land carbon cycle, including
97 photosynthesis, plant/soil respiration, carbon allocation, and tree growth. Simulated
98 carbon fluxes has been fully validated with carbon fluxes from 145 flux tower sites and
99 multiple satellite products (Yue and Unger, 2015). The YIBs model provides a unique
100 tool to identify drivers of decadal trends in carbon fluxes and BVOC emissions because
101 of the distinct treatments of plant phenology and BVOC emissions. Many state-of-art
102 vegetation models suffer from poor representations of phenology, which may lead to
103 large biases in the simulated carbon fluxes (Richardson et al., 2012). The optimized
104 phenology in YIBs is based on assessment of 13 existing models (9 for spring and 4 for
105 autumn), and has been validated against both ground-based records and multiple satellite

106 retrievals (Yue et al., 2015). In addition, YIBs incorporates two independent isoprene
107 emission schemes within the exact same host model framework (Unger et al., 2013;
108 Zheng et al., 2015) (i) a photosynthesis-dependent isoprene emission scheme (Niinemets
109 et al., 1999), and (ii) the Model of Emissions of Gases and Aerosols from Nature
110 (MEGAN) isoprene scheme (Guenther et al., 2012) that is widely used in chemistry-
111 transport modeling. Therefore, the YIBs model allows us to investigate modeling
112 uncertainties due to the differences in the BVOC emission algorithms themselves. The
113 major goals of this study are to identify: (1) the dominant drivers of the 30-year trends in
114 carbon fluxes and BVOC emissions from elevated CO₂, changes in meteorology
115 (temperature, radiation, and soil moisture), and human land use change; (2) the feedback
116 of biosphere, including changes in phenology and leaf area index (LAI), to the trends of
117 land carbon uptakes and BVOC emissions; and (3) the discrepancies in BVOC trends due
118 to application of different isoprene emission schemes.

119

120

121 **2 Data and methods**

122

123 **2.1 Observations and benchmark products**

124

125 We use long-term global measurements of LAI, GPP, and NPP to validate the simulated
126 trends. The LAI dataset for 1982-2011 is retrieved based on the Normalized Difference
127 Vegetation Index (NDVI) from Global Inventory Modeling and Mapping Studies
128 (GIMMS) with 1/12 degree resolution and a 15-day interval (Zhu et al., 2013). We also
129 use LAI data for 2000-2011 from the MODIS (<http://modis.gsfc.nasa.gov/>). GPP
130 benchmark products of 1982-2011 are upscaled from the FLUXNET eddy covariance
131 measurements using an ensemble of regression trees (Jung et al., 2009). As a comparison,
132 we also use the GPP and NPP datasets for 2000-2011 from the MODIS, which have been
133 developed based on remote sensing of biome parameters and assimilated meteorology
134 (Zhao et al., 2005). All the datasets are interpolated to the monthly interval at the 1°×1°
135 off-line YIBs model resolution.

136

137 **2.2 Model**

138

139 The YIBs model is a process-based terrestrial vegetation model that simulates the land
140 carbon budget and dynamic tree growth (Yue and Unger, 2015). The model adapts
141 routines from the mature TRIFFID (Cox, 2001) and CASA (Schaefer et al., 2008) models
142 with special updates in the parameterizations of ozone vegetation damage (Yue and
143 Unger, 2014), plant phenology (Yue et al., 2015), and the photosynthesis-dependent
144 isoprene emission (Unger et al., 2013). The model simulates carbon uptake for 9 plant
145 functional types (PFTs) including tundra, C3/C4 grass, shrubland, deciduous broadleaf
146 forest (DBF), ENF evergreen needleleaf forest (ENF), evergreen broadleaf forest (EBF),
147 and C3/C4 cropland. The vegetation biophysics calculates leaf-level photosynthesis using
148 the well-established Farquhar scheme (Farquhar et al., 1980; von Caemmerer and
149 Farquhar, 1981) and the stomatal conductance model of Ball and Berry (Collatz et al.,
150 1991). The canopy radiative transfer scheme computes direct and diffuse
151 photosynthetically active radiation (PAR) for sunlit and shaded regions for an adaptive
152 number of layers. The leaf photosynthesis is then integrated over all canopy layers to
153 generate the GPP.

154

155 Part of the assimilated carbon is used for maintenance and growth respiration, and the
156 rest is allocated among different pools for plant development. The model calculates
157 phenology for deciduous forests using cumulative temperature summation with additional
158 constraints from chilling and photoperiod (Yue et al., 2015). The phenology of shrubland
159 and grassland is jointly determined by the temperature- and drought-dependent metrics.
160 The LAI is then updated daily based on phenology and the net carbon assimilation. The
161 soil respiration scheme considers carbon flows among 12 biogeochemical pools,
162 including 3 live pools and 9 dead pools. The land carbon source or sink is calculated as
163 the difference between the net carbon assimilation and soil respiration.

164

165 The YIBs model incorporates two independent leaf-level isoprene emission schemes
166 embedded within the exact same host model framework (Zheng et al., 2015). The
167 photosynthesis-based (PS_BVOC) isoprene scheme calculates emissions based on the

168 electron transport-limited photosynthesis rate, canopy temperature, and intercellular CO₂
169 concentrations (Niinemets et al., 1999; Arneth et al., 2007; Unger et al., 2013). The
170 MEGAN scheme applies commonly used leaf-level empirical functions of light and
171 canopy temperature (Guenther et al., 1993). Both schemes implement CO₂ inhibition
172 effects on BVOC emissions parameterized as a reciprocal empirical function of
173 intercellular [CO₂] following the observations from Possell et al. (2005). For
174 monoterpene emissions, the YIBs model applies the same temperature-dependent scheme
175 as Lathiere et al. (2006) but with CO₂-inhibition effects. The leaf-level BVOC emissions
176 are integrated over the multiple canopy layers following the same approach as GPP to
177 obtain the total canopy-level emissions.

178

179 YIBs can be used in three different configurations with increasing complexity: (1) off-
180 line local site level, which is driven with hourly measurements of CO₂ concentrations and
181 meteorology at flux tower sites; (2) off-line global forced with spatially uniform but
182 annually updated CO₂ concentrations and hourly gridded reanalysis meteorology; (3) on-
183 line coupled to the NASA ModelE2 driven with simulated meteorology by the GCM
184 every half hour. At the site level, YIBs simulates reasonable seasonality (correlation
185 coefficient $R > 0.8$) of GPP at 121 out of 145 flux-tower sites with biases in magnitude
186 ranging from -19 to 7 % depending on PFTs. On the global scale, the offline model
187 simulates an annual GPP of 125 ± 3 Pg C and net ecosystem exchange (NEE) of $-2.5 \pm$
188 0.7 Pg C for 1982-2011, with seasonality and spatial distribution consistent with both
189 satellite observations and benchmark synthesis products (Yue and Unger, 2015).
190 However, the model does not include a fully coupled carbon-nitrogen cycle, which may
191 overestimate CO₂ fertilization effects. In addition, phenology of evergreen trees is set to
192 constant value of 1, leading to underestimation of phenological feedbacks to flux trends.
193 In this study, we use the (2) off-line global version of the model, which is driven with
194 global meteorology reanalysis data and observed CO₂ concentrations.

195

196 **2.3 Simulations**

197

198 We apply observed historical atmospheric CO₂ concentrations from the fifth assessment
199 report (AR5) of the Intergovernmental Panel on Climate Change (IPCC) (Meinshausen et
200 al., 2011). We apply an annually-varying historical transient land cover dataset (Oleson et
201 al., 2013), which is developed based on a combination of remote sensing data from both
202 MODIS (Hansen et al., 2003) and the Advanced Very High Resolution Radiometer
203 (AVHRR) (Defries et al., 2000), and with land use change from Hurtt et al. (2011). We
204 use hourly meteorological variables for 1980-2011 from the WATCH Forcing Data
205 methodology applied to ERA-Interim data (WFDEI, Weedon et al., 2014). The WFDEI
206 reanalysis is an update of the WATCH Forcing Data (WFD), which is developed based
207 on the European Centre for Medium-range Weather Forecasts (ECMWF) ERA-40
208 reanalysis (Uppala et al., 2005). Meteorological variables applied include surface air
209 temperature, specific humidity, wind speed, surface pressure, total PAR, and soil
210 temperature and wetness. All of the forcing data are interpolated to the 1°×1° model
211 resolution at the hourly interval.

212

213 We perform 10 sensitivity simulations to distinguish driving factors for the changes in
214 land carbon fluxes and BVOC emissions in the past 3 decades (Table 1). The control
215 simulation (CO2_MET_LUC) uses interannually-varying meteorology, [CO₂], and land
216 cover for 1980-2011. The CO2_MET run is the same as the control simulation but
217 prescribes land cover at the year 1980. Three single-factor runs prescribe most boundary
218 conditions at the year 1980 but allow the interannual variations of [CO₂] (CO2_ONLY),
219 land cover (LUC_ONLY), and meteorology (MET_ONLY) respectively. Results from
220 these runs are compared with that of control simulation to determine the dominant drivers
221 of simulated trends. To understand the impact of individual meteorological variables,
222 three additional runs are performed with fixed (or recycled) [CO₂], land cover, and all
223 meteorology at year 1980 but one field varying for 1980-2011 each time, including
224 temperature (TEMP_ONLY), PAR (PAR_ONLY), and soil wetness (SOILW_ONLY).
225 Finally, two runs are performed to examine feedback of biospheric changes. LAI_ONLY
226 prescribes all boundary conditions at the starting year 1980 but implements the year-to-
227 year LAI simulated by the control run. PHEN_ONLY also prescribes all forcings at the
228 starting year except for the year-to-year phenology from control simulation. All

229 simulations are initialized following the same spin up process (Yue and Unger, 2015) and
230 are integrated for 1980-2011.

231

232

233 **3 Results**

234

235 **3.1 Drivers of trends in LAI**

236

237 Observations show an increasing trend of LAI on most of vegetated continents, especially
238 in Europe, northern and eastern Asia, central Africa, and southeastern U.S. in the past 3
239 decades (Fig. 1a). The simulation with year-to-year [CO₂], land cover, and meteorology
240 reproduces the magnitude of trend in Europe and the sign of trend in northern Asia,
241 eastern U.S., central Asia, and Australia (Fig. 1b). The model predicts negative changes
242 in central Africa, western U.S., eastern Asia, and the east of South America, which are
243 inconsistent with satellite observations. These negative trends are mainly contributed by
244 the changes in meteorology (Fig. 1e), except for that in East Asia where land cover
245 changes due to human activities result in the decline of LAI (Fig. 1f). Without the land
246 use perturbation, the negative LAI trend in East Asia is weakened and the prediction is
247 closer to observations (Fig. 1c). For the individual drivers, CO₂ fertilization leads to
248 widespread increases in LAI (Fig. 1d), meteorology causes dipole changes on most
249 continents (Fig. 1e), and land use change generally results in negative trends (Fig. 1f).
250 Regionally, simulation CO₂_MET_LUC shows a positive trend of 0.0035 m² m⁻² a⁻¹ in
251 Europe (Table 2), close to the observed value of 0.0049 m² m⁻² a⁻¹ (Fig. 1a). In other
252 areas, simulated LAI trends are either underestimated (by 87% in Amazon, 78% in North
253 America, and 48% in Central Africa) or opposite in sign (East Asia and Indonesia)
254 compared to observations. Such inconsistencies indicate the limit of model simulations,
255 but may also in part result from the uncertainties in the satellite measurements (see
256 section 4.1).

257

258 **3.2 Drivers of trends in land carbon fluxes**

259

260 Predicted GPP and NPP trends show similar spatial pattern as that of LAI (Figs. 2a and
261 2c). However, regional trends are all positive in the main continents and on the global
262 scale (Tables 2 and 3). Tropical areas are experiencing maximum changes, especially in
263 Central Africa (GPP by 83.3 Tg C a⁻² and NPP by 51.7 Tg C a⁻²) and the Amazon (52.7
264 and 27.1 Tg C a⁻²). In the Northern Hemisphere (NH), changes are significant in Europe
265 (53.4 and 33.2 Tg C a⁻²), East Asia (42.4 and 27.2 Tg C a⁻²), and North America (13.6
266 and 9.7 Tg C a⁻²). 30-year historical observations of GPP and NPP are not available.
267 Therefore, we compare YIBs predictions with MODIS land carbon fluxes over the more
268 recent period of 2000-2011 (Fig. 3). Different from the 30-year trend, land carbon fluxes
269 over the recent decade show negative trends in southeastern U.S., southern Africa,
270 eastern Australia, and central and northern Asia (Figs. 3a and 3c). Most of these changes
271 are consistent with the MODIS observations (except for the U.S., Figs. 3b and 3d) and
272 are attributed to the drought tendency in the past decade (Zhao and Running, 2010).

273

274 For the 30-year trend, both CO₂ and meteorology are playing important roles (Figs. 2b
275 and 2d). CO₂ fertilization dominates the GPP and NPP trends of tropical forests in the
276 Amazon, central Africa, and Indonesia, and ENF and DBF in boreal North America,
277 eastern Europe, and central and northern Asia. Land use change plays a limited role in
278 land carbon cycle flux trends over the past 3 decades, except for some areas in northern
279 Africa. Meteorological forcing drives changes in land carbon fluxes for tundra in
280 subarctic regions, C3 grasslands in the central U.S. and southern Africa, C4 grasslands in
281 central Africa and the east of South America, and shrublands in Australia and southern
282 Asia. Soil wetness plays the dominant role in the tropical and subtropical areas (Fig. 4b).
283 The drought tendency in the western U.S., central Africa, and the east of South America
284 (Fig. S1d) results in the regional decline of land carbon fluxes (Fig. 4a). In contrast, the
285 increasing wetness in the northern Amazon and southern Africa leads to the enhancement
286 of regional GPP. Warming is the main cause for the GPP trends over the subarctic areas
287 (Fig. 4b). Contribution of PAR is limited, except for some areas in the eastern Europe.

288

289 The simulated net ecosystem productivity (NEP) shows weaker trends compared with
290 GPP and NPP (Fig. 2e), because NEP is offset by the significant trends in heterotrophic

291 respiration (Rh) (Table 2). Regionally, the YIBs model predicts enhanced net land carbon
292 uptake in boreal North America, northern Asia, and southern Africa but reduced NEP in
293 the central U.S., the Amazon, central Africa, eastern Europe, and East Asia. The
294 simulated global NEP trends (Fig. 5d) are in broad agreement with the comprehensive
295 bottom-up estimates by Pan et al. (2011), who found slightly decreasing net carbon
296 uptake by global established forests (without human perturbations in the tropics but with
297 afforestation in subtropical areas) in 2000-2007 relative to that in 1990-1999. Attribution
298 analysis shows that the NEP trends are mainly driven by the changes in meteorological
299 forcings (Fig. 2f), because CO₂ fertilization enhances both NPP and Rh with similar
300 magnitude (Fig. 5).

301

302 On the global scale, GPP, NPP, and Rh increase respectively by 298, 185, and 181 Tg C
303 a⁻² in the past 3 decades (Table 3). The long-term trends of carbon fluxes are mainly
304 driven by CO₂ fertilization, while the interannual variability is related to meteorological
305 forcings (Fig. 5). Warming alone decreases GPP especially in tropical forests (not shown)
306 but increases autotrophic respiration (Ra), leading to global reductions of 56 Tg C a⁻² in
307 NPP and 10 Tg C a⁻² in NEP (Table 3). Drought alone strongly decreases GPP, especially
308 for tropical grassland and shrubland (Fig. 4), leading to reductions of 51 Tg C a⁻² in NPP
309 and 13 Tg C a⁻² in NEP. Trends in PAR do not affect GPP and NPP, but may decrease
310 NEP by 23 Tg C a⁻² because soil respiration is slowly increasing to reach the equilibrium.
311 Land use change has very limited impacts on the trends of carbon fluxes, though it
312 induces relatively large reductions in NEP (Table 3).

313

314 **3.3 Drivers of trends in BVOC emissions**

315

316 Simulated isoprene emission trends are sensitive to the choice of modeling scheme. With
317 the PS_BVOC scheme, global isoprene emissions increase by 0.4 Tg C a⁻² during 1982-
318 2011. Large enhancements are predicted in central Africa (0.25 Tg C a⁻²) and Europe
319 (0.16 Tg C a⁻²), while moderate reductions are found in the western U.S., eastern South
320 America, and East Asia (Fig. 6a). Drought accounts for the decline of isoprene emissions
321 in the U.S. and South America, but land use change is the main driver for the reductions

322 in East Asia (Fig. 6b). Increasing $[\text{CO}_2]$ promotes photosynthesis but meanwhile inhibits
323 BVOC emissions, leading to offsetting CO_2 effects on isoprene. Consequently, the global
324 isoprene emission is mainly driven by meteorological changes (Fig. 6b). In contrast,
325 using MEGAN scheme, the YIBs model simulates a global reduction of 1.1 Tg C a^{-2} for
326 isoprene emissions (Fig. 6c). Strong declines are found in the tropical rainforest, for
327 example in the Amazon ($-0.43 \text{ Tg C a}^{-2}$), central Africa ($-0.14 \text{ Tg C a}^{-2}$), and Indonesia ($-$
328 0.16 Tg C a^{-2}) (Fig. 6c). The MEGAN scheme is sensitive to both light and temperature
329 (Guenther et al., 1995). The strong positive brightening trends in PAR in Europe (Fig.
330 S1b) promote isoprene emissions there. The positive impacts of NH warming (Fig. S1a)
331 are compensated by CO_2 inhibition, leading to small changes in isoprene emissions (Fig.
332 6c). In the tropical areas, where trends of temperature and PAR are limited, CO_2
333 inhibition results in strong reductions of BVOC emissions. Monoterpene emissions show
334 a global reduction of 0.04 Tg C a^{-2} over the past 3 decades (Fig. 6e).

335

336 **3.4 Feedback of biospheric changes to the trends**

337

338 Due to the changing climate and CO_2 fertilization, the biosphere is experiencing
339 significant changes in the past 3 decades. The most evident alterations include LAI
340 changes in peak season and phenological changes in growing and falling seasons. In this
341 section, we explore the feedback of these biospheric changes to the carbon uptake and
342 BVOC emissions.

343

344 **3.4.1 Impacts of LAI changes**

345

346 Sensitivity run LAI_ONLY retains the trends in LAI but prescribes other forcings. In this
347 simulation, trends in GPP (Fig. S2a) and NPP (Fig. S2c) generally follow that in LAI
348 (Fig. 1b), but with smaller magnitude relative to those in control simulations (Figs. 2a
349 and 2c). LAI in the north of 30°N shows widespread increases in both observations and
350 simulations (Figs. 1a and 1b). Over these northern lands, the unit change in leaf area
351 leads to enhancement of regional GPP by 32 Pg C a^{-1} , much lower than the response of
352 $116 \text{ Pg C a}^{-1} \text{ LAI}^{-1}$ for the simulation including CO_2 fertilization and climate forcings

353 (Fig. 7a). In the tropical areas, both positive and negative LAI trends are predicted due to
354 the competition between CO₂ fertilization and drought effects (Fig. 1). As a result, LAI-
355 induced GPP and NPP changes show patchy distributions at tropics (Fig. S2a and S2c),
356 leading to moderate changes in the global carbon assimilations (Table 3).

357

358 Trends in isoprene emission (calculated with the PS_BVOC scheme) also follow that of
359 LAI, except that leaf expansion results in decreased emissions at high latitudes (~60°N,
360 Fig. S2e). The cause for such inconsistency is unclear, but might be because the denser
361 leaves reduce radiation penetrating to lower canopy layers. Such impact would only
362 affect BVOC emissions at high latitudes because PAR is usually limiting near subarctic
363 areas. In most of the subtropical areas, increased LAI leads to enhanced isoprene
364 emissions. On average, unit change in LAI at north of 30°N leads to enhanced isoprene
365 emissions by 43 Tg C a⁻², only 25% of the magnitude in simulation CO₂_MET (Fig. 7b).
366 A similar ratio of 23% is achieved for MEGAN isoprene emissions. These results are
367 consistent with that for GPP (Fig. 7a), suggesting that CO₂ fertilization and
368 meteorological changes are the main drivers for the changes in carbon uptake and BVOC
369 emissions, even over the northern lands where the most evident changes in LAI are
370 observed.

371

372 **3.4.2 Impacts of phenological changes**

373

374 Plant phenology, which is the timing of budburst and leaf fall, is closely related to
375 temperature, moisture, and photoperiod and thus is experiencing significant changes in
376 the past decades following climate change (Jeong et al., 2011; Keenan et al., 2014;
377 Buitenwerf et al., 2015; Yue et al., 2015). Extension of the growing season has the
378 potential to promote carbon uptake of forests (e.g., Piao et al., 2007; Richardson et al.,
379 2009). Yet such inference requires careful interpretation because the phenological
380 changes are usually accompanied with warming and elevated [CO₂], both of which are
381 also contributing to the enhancement of carbon fluxes. Phenological changes are also
382 expected to affect BVOC emissions, however, such investigations are still missing
383 (Richardson et al., 2013). With the YIBs model, we evaluate the impacts of the growing

384 season extension on both carbon uptake and BVOC emissions by isolating long-term
385 phenological trends from changes in temperature and [CO₂].

386

387 The YIBs model simulates advanced spring and delayed autumn over most areas in NH
388 (Fig. S3). Budburst dates advance on average by 0.16 days a⁻¹ in Europe and 0.15 days a⁻¹
389 in East Asia (Table 2), but with moderate changes or even delays in northwestern Asia
390 and eastern Siberia (Fig. S3a). Spring is earlier by 0.14 days a⁻¹ in eastern U.S. while
391 delayed by 0.15 days a⁻¹ in northwestern U.S. and southeastern Canada, leading to a
392 minor advance of 0.01 days a⁻¹ over North America. Dormancy onset dates are largely
393 delayed in eastern Europe and northwestern Asia (~0.3 day a⁻¹), western U.S. (~0.1 day a⁻¹)
394), boreal Canada (~0.1 day a⁻¹), and northeastern China (~0.1 day a⁻¹) (Fig. S3b).
395 Advanced autumn (~0.1 day a⁻¹) is predicted in northern Asia. Most of these changes are
396 consistent with observations from remote sensing data (Jeong et al., 2011), except for
397 some discrepancies in the magnitude. The predicted phenological trends mainly follow
398 the long-term changes of surface air temperature, especially that in April (for spring) and
399 September (for autumn) (Fig. S4). Sensitivity tests without chilling requirement and
400 photoperiod limit show similar changes (Yue et al., 2015), suggesting that temperature
401 changes dominantly drive the trends of forest phenology in the past 3 decades.

402

403 On average, the YIBs model simulates advanced budburst by 0.12 day a⁻¹ and delayed
404 dormancy onset by 0.09 day a⁻¹ at north of 30°N in the past 3 decades (Figs. 8a and 8b).
405 Observations based on remote sensing greenness show trends of -0.11 day a⁻¹ for onset
406 and 0.25 day a⁻¹ for offset during 1990-2009 (Zhu et al., 2013). An ensemble prediction
407 based on 9 terrestrial models yields an advance of 0.08 ± 0.13 day a⁻¹ for onset and a
408 delay of 0.22 ± 0.1 day a⁻¹ for offset (Sitch et al., 2015). Our predictions are in broad
409 agreement with these estimates though the autumn delay is less, likely because the
410 positive trend of offset is weaker for the recent decade (Jeong et al., 2011).

411

412 We plot the annual total GPP and isoprene emissions at north of 30°N against the length
413 of growing season for 1982-2011 (Figs. 8c and 8d). In the CO₂_MET run, the 1-day
414 extension is correspondent to increases of 0.17 Pg C a⁻¹ in GPP and 0.34 Tg C a⁻¹ in

415 isoprene emissions. If only temperature is allowed to vary, the phenological trend
416 remains the same while the increases of GPP and isoprene emissions are largely
417 weakened. In the TEMP_ONLY run, the 1-day extension in growing season is
418 accompanied by increases of 0.05 Pg C a⁻¹ in GPP and 0.25 Tg C a⁻¹ in isoprene
419 emissions. The changes in BVOC emissions are not as dramatic as those of GPP because
420 CO₂ has both enhancing and suppressing impacts on the former. If we further exclude
421 temperature effects (PHEN_ONLY run), GPP increases only by 0.01 Pg C a⁻¹ while
422 isoprene emissions decrease by 0.1 Tg C a⁻¹, both of which are not statistically
423 significant, suggesting that the phenological change alone does not promote either GPP
424 or isoprene emissions. There are two reasons for this apparent contradiction. First, the
425 extension of the growing season occurs in shoulder months, usually in May and
426 September, when both GPP and BVOC emissions and their changes are much smaller
427 compared to that in peak months (Fig. S5). Second, phenological changes are not uniform
428 in space. As Fig. S3 shows, both positive and negative changes are predicted for budburst
429 and dormancy onset dates. Such spatial inhomogeneity, in combination with the
430 discrepancies in regional vegetation types and meteorological conditions, result in varied
431 responses in GPP (Fig. S2b) and isoprene emissions (Fig. S2f).

432

433 Plant phenology at lower latitudes (30°S-30°N) is also experiencing dramatic changes,
434 though such changes are diverse in phase, magnitude, or both (Buitenwerf et al., 2015).
435 In the model, tropical phenology is mainly driven by soil wetness and as a result exhibits
436 large changes in the past 3 decades (not shown). These changes lead to a reduction of 42
437 Tg C a⁻¹ in GPP at the tropics (Fig. S2b), which accounts for 14% of global GPP trend
438 but with the opposite sign (Table 3), suggesting additional inhibition of drought on
439 carbon cycle. A similar conclusion applies for BVOC emissions (Fig. S2f), though
440 experiments suggest that isoprene production has some tolerance to mild drought
441 conditions (e.g., Pegoraro et al., 2006). However, changes in drought-dependent
442 phenology are very uncertain and observations are not available for evaluation. We
443 assume that phenological changes may have larger impacts on both carbon assimilation
444 and BVOC emissions at tropical areas than that at higher latitudes.

445

446

447 **4 Discussion**

448

449 **4.1 Uncertainties in observations**

450

451 Terrestrial biosphere modeling is a useful tool to identify drivers of long-term changes in
452 land carbon fluxes. The reliability of simulations is dependent on the availability of
453 observations for model validation. In this study, we use 30-year LAI observations from
454 the LAI3g product (Zhu et al., 2013) and 12-year GPP from MODIS (Zhao et al., 2005),
455 both of which are remote sensing retrievals, to validate the simulated trends (Figs. 1 and
456 3). We found the offline global model biases against both fields, especially for LAI (Fig.
457 1). Such discrepancies may in part result from the uncertainties in measurements
458 themselves. As a check, we compare the derived LAI trends from LAI3g with retrievals
459 from MODIS for the overlap period of 2000-2011 (Figs. S6a and S6b). Global LAI
460 significantly increases in LAI3g but show widespread reductions in MODIS, especially
461 over subtropical areas. Simulated trends (CO2_LUC_MET) are closer to the estimates
462 with MODIS, especially for the changes in the NH (not shown). Meanwhile, we compare
463 the derived GPP trends from MODIS with that upscaled from FLUXNET data using an
464 ensemble of regression trees (Jung et al., 2009) for 2000-2011 (Figs. S6c and S6d). The
465 two products show similar trends over most areas except for some discrepancies in
466 tropical areas and the eastern U.S. Simulated GPP trends match results from Jung et al.
467 (2009) better than that from MODIS (Fig. 3a). However, we do not use Jung et al. (2009)
468 to validate simulations for 1982-2011 because the earliest flux tower observations began
469 only in middle 1990s. The large discrepancies in the observed trends among different
470 data sets not only indicate the importance of model evaluations with multiple products,
471 but also put forward the necessity of data inter-comparisons and algorithm improvements
472 to alleviate uncertainties in observations.

473

474 **4.2 Comparisons with other modeling studies**

475

476 We assess the YIBs simulations within the context of other models and/or previous multi-
477 model studies to evaluate the robustness of the predicted trends in land carbon fluxes and
478 BVOC emissions. The YIBs model predicts NPP trends of 67.4 Tg C a^{-2} in northern land
479 ($25\text{-}90^\circ\text{N}$) and 98.1 Tg C a^{-2} in tropical land ($15^\circ\text{S}\text{-}25^\circ\text{N}$), similar to the ensemble
480 estimates of 63 ± 22 and $102 \pm 34 \text{ Tg C a}^{-2}$ for 1990-2009 based on 9 terrestrial biosphere
481 models (Sitch et al., 2015). However, the simulated NPP trend is only 19.8 Tg C a^{-2} in
482 southern land ($15\text{-}90^\circ\text{S}$), much lower than the ensemble mean value of $53 \pm 31 \text{ Tg C a}^{-2}$
483 in Sitch et al. (2015). As for the NEP, the YIBs predicts trends of 2.0 Tg C a^{-2} in northern
484 land, 1.0 Tg C a^{-2} in tropical land, and -0.3 Tg C a^{-2} in southern land, much smaller in
485 magnitude compared with the -2.0 ± 12 , 36.0 ± 13 , and $21 \pm 17 \text{ Tg C a}^{-2}$ estimated by
486 Sitch et al. (2015). However, their predictions are insignificant ($p > 0.05$) for 9, 5, and 7
487 out of 9 models in the northern, tropical, and southern land respectively, suggesting that
488 the strengthening uptake by terrestrial ecosystem is not robust.

489
490 For the BVOC, Stavrakou et al. (2014) investigated isoprene emissions over Asia during
491 1979-2012 using the MEGAN scheme and taking into account both climate and land-use
492 changes. Their results showed widespread increases in the emissions over China but
493 moderate decreases in Indonesia. In contrast, the YIBs model with the MEGAN scheme
494 simulates widespread reductions in the same areas for 1980-2011 (Fig. 6c). The
495 discrepancies between studies are accounted for by differences in the drivers including
496 land cover change, meteorology, and CO_2 inhibition effects. The YIBs model is driven
497 with land cover data from Hurtt et al. (2011), which estimates an increase of crop (non-
498 isoprene emitter) fraction in East China by 0.32% per year in the last 3 decades, at the
499 cost of the coverage loss by $0.12\% \text{ a}^{-1}$ for DBF and $0.14\% \text{ a}^{-1}$ for ENF (strong BVOC
500 emitters). However, the data from Ramankutty and Foley (1999), used by Stavrakou et al.
501 (2014) with updates to 2007, show a reduction of the crop fraction over East China for
502 the similar period. In addition, the ERA-Interim PAR used in Stavrakou et al. (2014)
503 shows an increasing trend in southeast China (c.f. their Fig. 5c). On the contrary, the
504 WFDEI PAR for YIBs exhibits a declining trend in the same region (Fig. S1b), leading to
505 a reduction in isoprene emissions. The WFDEI surface solar radiation is based on the
506 ERA-Interim radiation but is adjusted using the average cloud cover from the Climatic

507 Research Unit (CRU) and taking into account the effects of interannual changes in
508 atmospheric aerosols (Weedon et al., 2011). Finally, the YIBs simulations include CO₂
509 inhibition effects on BVOC emissions, which were neglected in Stavrakou et al. (2014).

510

511 Naik et al. (2004) predicted a global trend of 1.3 Tg C a⁻² for isoprene emissions during
512 1971-1990 using the Integrated Biospheric Simulator (IBIS) driven with monthly mean
513 CRU meteorology. Lathiere et al. (2006) estimated an increasing global trend of 0.3 Tg C
514 a⁻² for 1983-1995 using the ORCHIDEE (Organizing Carbon and Hydrology in Dynamic
515 EcosystEms) vegetation model driven with sub-daily variables from the NCEP/DOE
516 (National Center for Environmental Predictions/Department of Energy) Reanalysis 2.
517 Muller et al. (2008) reported a global increase of 4.5 Tg C a⁻² for 1995-2006 using a
518 canopy environmental model and the NCEP meteorological data. In contrast to these
519 previous studies, YIBs with the MEGAN scheme simulates a decreasing trend of ~1 Tg C
520 a⁻² in the past 3 decades. The main cause of the discrepancy in the sign of change is the
521 missing CO₂ inhibition effects in the previous studies. In addition, differences in
522 vegetation models, meteorological forcings, and time frames of investigation also likely
523 contribute. The YIBs result is consistent with a recent study by Sindelarova et al. (2014),
524 who reported a decreasing trend of ~1.2 Tg C a⁻² for global isoprene emissions during
525 1980-2010 using the MEGAN scheme and inclusion of a CO₂ inhibition parameterization
526 from Heald et al. (2009).

527

528 **4.3 Impacts of CO₂ effects**

529

530 Similar to the multi-model ensemble predictions (Sitch et al., 2015), we found that global
531 trends in carbon fluxes are dominantly driven by CO₂ fertilization (Figs. 2 and 5). In the
532 YIBs, the global responses to elevated [CO₂] is 0.2% ppm⁻¹ for GPP and 0.27% ppm⁻¹ for
533 NPP, with relatively uniform spatial distribution (Figs. S7a and S7b). The GPP response
534 falls within the range of 0.05-0.21% ppm⁻¹ predicted by 10 terrestrial models (Piao et al.,
535 2013) and that of 0.01-0.32% ppm⁻¹ observed from multiple free-air CO₂ enrichment
536 (FACE) sites (Ainsworth and Long, 2005). The NPP response is higher than the model
537 ensemble of 0.16% ppm⁻¹ (Piao et al., 2013) and the observed median value of 0.13%

538 ppm⁻¹ (Norby et al., 2005), suggesting that CO₂ fertilization to NPP may be
539 overestimated in the YIBs. One possible cause is the omission of N limitation in the
540 model, which could reduce CO₂ responses by half (Piao et al., 2013). Elevated [CO₂]
541 leads to increases of 0.023 Pg C a⁻¹ ppm⁻¹ in NEP, within the multi-model range of 0.003-
542 0.06 Pg C a⁻¹ ppm⁻¹ (Piao et al., 2013).

543

544 Responses of BVOC emissions to elevated [CO₂] are different between PS_BVOC and
545 MEGAN schemes (Figs. S7c and S7d). PS_BVOC includes both CO₂ fertilization (on
546 photosynthesis) and inhibition (on isoprene) effects, leading to moderate but generally
547 positive changes in isoprene emissions. In contrast, emissions from the MEGAN scheme
548 are not dependent on foliar photosynthesis and as a result only CO₂ inhibition is enforced.
549 Chamber experiments show contrary tendencies for photosynthesis and isoprene in
550 response to elevated [CO₂] (Possell et al., 2005), supporting the simulations with
551 MEGAN. In addition, the magnitude of CO₂ inhibition implemented in MEGAN (-0.25%
552 ppm⁻¹) is close to observations (-0.26% ppm⁻¹) in Possell et al. (2005). However, most of
553 these experiments are conducted for short-term period and cannot detect LAI changes due
554 to the long-term CO₂ fertilization. In addition, the impacts of CO₂ are dependent on
555 species and environmental conditions (ambient temperature and light availability). For
556 example, Buckley (2001) found almost no responses in isoprene emissions to the elevated
557 [CO₂] for oak trees. Furthermore, experiments with high temperature and/or light density
558 show increasing isoprene at elevated [CO₂] (Sun et al., 2013). These studies suggest that
559 the real responses of isoprene emissions to CO₂ under long-term climate change may not
560 be so linear as predicted in MEGAN scheme. More sensitivity experiments and long-term
561 samplings are required to identify CO₂-isoprene relationships on broad range of biomes
562 and locations.

563

564 **4.4 Impacts of meteorology**

565

566 Predicted long-term trends show large deviations against observations at tropical areas
567 (Fig. 3), where meteorology plays important and complex roles. Responses of carbon
568 fluxes to temperature are more diverse than to CO₂ (Figs. S8a and S8b). In the YIBs,

569 negative responses of GPP and NPP are predicted in tropical areas, where soil moisture
570 availability limits plant functions (e.g. stomatal conductance) to the increased
571 temperature. Furthermore, for tropical rainforests where ambient temperature is higher
572 than optimal photosynthetic temperature (25-30°C), additional warming decreases carbon
573 assimilation, especially for NPP because of simultaneous increases in plant respiration
574 (Liang et al., 2013). On the contrary, warming leads to enhanced GPP and NPP at wetter
575 and cooler areas in the NH subtropics. Such spatial pattern is consistent with multi-model
576 ensemble predictions (Piao et al., 2013). On the global scale, warming results in changes
577 of -0.7% °C⁻¹ for GPP in YIBs, falling within the range of -1.6-1.4% °C⁻¹ estimated by 10
578 models (Piao et al., 2013). Predicted NPP responses of -15-6% °C⁻¹ (Fig. S8b) is not so
579 positive as the measurements of -8-40% °C⁻¹, probably because most of current warming
580 experiments are located in subtropics of NH (Wu et al., 2011). Elevated temperature
581 changes NEP by -1.4 Pg C a⁻¹ °C⁻¹, also within the multi-model range of -5~-1 Pg C a⁻¹
582 °C⁻¹ (Piao et al., 2013). Simulated isoprene emissions with PS_BVOC show similar
583 warming responses as that of carbon fluxes (Fig. S8c), except for tropical rainforests
584 where the former is positive while the latter is negative. Such decoupling is attributed to
585 the differences in optimal temperatures between isoprene (35-40 °C) and photosynthesis
586 (25-30 °C). Simulations with MEGAN scheme show very strong temperature dependence
587 of 6-15% °C⁻¹ (Fig. S8d), consistent with measurements of 5-20% °C⁻¹ for aspen
588 (Niinemets and Sun, 2015) and 9-12% °C⁻¹ for oak (Li et al., 2011). However,
589 experiments with some other species (e.g. spruce in Kivimaenpaa et al. (2013)) show no
590 responses or moderate ones, suggesting that warming sensitivity of isoprene emissions
591 might be dependent on species and ambient conditions.

592

593 Responses to PAR are mostly positive and distributed evenly, with global sensitivity of
594 0.3% W⁻¹ m² for GPP and 0.5% W⁻¹ m² for NPP (Figs. S9a and S9b). Isoprene emissions
595 from both PS_BVOC and MEGAN schemes show similar responses to PAR, with larger
596 sensitivity in subtropics than that in tropics (Figs. S9c and S9d), likely because the
597 ambient PAR is higher at lower latitude, leading to slower responses of isoprene
598 emissions to the unit changes of light (Guenther et al., 1993). YIBs simulations show that

599 PAR is not the driver of long-term trends in carbon fluxes and BVOC emissions (Fig. 4),
600 likely because changes in solar radiation is limited in the past 3 decades (Figs. S1b).

601

602 Soil moisture dominates climate-driven flux changes in tropical areas (Fig. 4). In YIBs
603 model, changes in soil water availability affect carbon assimilation through the alteration
604 of leaf stomatal conductance and plant phenology (especially for shrublands and
605 grasslands in arid regions). Both GPP and NPP show strong responses to soil wetness
606 variations, especially over tropics where >10% changes are found for every increase of
607 0.01 in soil wetness at 1.5 m (Figs. S10a and S10b). On the global scale, GPP changes by
608 4.7% 0.01^{-1} and NPP by 5.5% 0.01^{-1} in response to soil wetness. Although experiments
609 also show rapid reductions in carbon assimilation due to drought stress (e.g., Ruehr et al.,
610 2012; Xia et al., 2014), the magnitude of such influence is difficult to evaluate because
611 different metrics and depths of soil water are used in measurements. Isoprene emissions
612 from PS_BVOC show similar soil-wetness responses to that of GPP (Fig. S10c),
613 indicating that drought reduces BVOC emissions. However, observations show
614 insignificant changes of isoprene with mild drought stress (e.g., Pegoraro et al., 2006),
615 though such drought tolerance is strongly weakened at severe drought and/or warm
616 conditions (Centritto et al., 2011). Consistent with these experiments, MEGAN scheme
617 does not include drought inhibition on isoprene emissions. Simulations with YIBs show
618 large responses of BVOC to soil wetness in tropical areas (Fig. S10d), mainly because of
619 the changes in drought-dependent phenology.

620

621 **4.5 Impacts of land use change**

622

623 Changes of land use show moderate impacts on global carbon budget (Fig. 2) and BVOC
624 emissions (Fig. 6) in the past 3 decades, though regional perturbations are found in China
625 and Europe. The afforestation in Europe helps promote regional carbon uptake, resulting
626 in more reasonable trends in LAI compared with remote sensing data (Fig. 1). However,
627 the expansion of crop in China leads to a reduction in LAI, which is not supported by the
628 satellite data. One possible cause is the uncertainty in crop fraction, because data from
629 Hurtt et al. (2011), used by YIBs, show crop expansion while data from Ramankutty and

630 Foley (1999) suggest reductions of the crop fraction over East China over the similar
631 period. The role of land use change in our simulation might be conservative because we
632 consider only land cover changes. Perturbed emissions from land use management, such
633 as forest lodging, cropping practice, use of fertilizer, fire management and so on
634 (Houghton, 2010) may alter regional carbon budget by changing carbon sinks to sources.
635 Studies including gross emissions of land use perturbation estimated a global net land
636 source to atmosphere, which shows decreasing trend in the last 3 decades (Ciais et al.,
637 2013). Such change may help strengthen net land carbon sink but is missing in our study.

638

639 **4.6 Impacts of biospheric changes**

640

641 The land biosphere has experienced significant changes in the past 3 decades. At north of
642 30°N, changes in LAI account for 25% of the trends in regional carbon fluxes and
643 isoprene emissions. However, the extension of growing season alone makes insignificant
644 contributions to the increased carbon assimilation. This conclusion is inconsistent with
645 site-level observations that show evident increases in carbon assimilation at early spring
646 and/or late autumn in recent decades (Dragoni et al., 2011; Keenan et al., 2014). The
647 causes for such discrepancies lie in two. First, phenology at specific location may exhibit
648 much more intense changes than that at larger scale. For example, Dragoni et al. (2011)
649 estimated extensions of growing season by 2.3-3.3 day a⁻¹ in Morgan-Monroe State
650 Forest in south-central Indiana of US for 1998-2008. The magnitude of this change is ~10
651 times larger than the observed value of 0.36 day a⁻¹ from satellite and simulated value of
652 0.22 day a⁻¹ with YIBs for the northern lands. Second, enhanced temperature also
653 contributes to the stronger uptake at early spring and late autumn. One difficulty for the
654 observation-based estimate of phenological impacts is that extension of growing season is
655 accompanied by warmer climate, which may stimulate both carbon assimilation and
656 BVOC production. In a recent study, Barlow et al. (2015) found invariant length of land
657 carbon uptake period at high northern latitudes based on the first time differential of
658 atmospheric CO₂ concentrations, suggesting that increased greenness is not necessarily
659 equal to enhanced carbon uptake in shoulder seasons. Furthermore, Barlow et al. (2015)
660 showed that enhanced peak uptake is the main driver for the strengthened carbon sink at

661 high northern latitudes over the past 4 decades. These conclusions are supportive of our
662 simulations for the monthly trends at subtropical regions (North America, Europe, and
663 East Asia) (Fig. S5).

664

665

666 **5 Conclusions**

667

668 With YIBs model, we estimated global increases of carbon assimilation especially at
669 tropical areas for 1982-2011. This trend is mainly attributed to the widespread CO₂
670 fertilization effect, and jointly affected by changes in meteorology and land cover.
671 Increase of temperature promotes carbon uptake of forest ecosystems at high latitudes
672 (>30°N) while drought tendency dampens GPP and NPP of grasslands and shrublands at
673 low latitudes (30°S-30°N). The widespread increases of LAI at northern lands account for
674 ~25% of the regional GPP trends. Significant changes in phenology are found at north of
675 30°N; however, this temperature-driven phenological change alone is not promoting
676 regional carbon assimilation. Changes in land use show limited influences on global
677 carbon fluxes, except for some regional impacts over Europe (afforestation) and China
678 (deforestation). Due to the simultaneous enhancement in soil respiration, land carbon sink
679 has remained almost stable in the past 3 decades. The YIBs model does not yet include a
680 fully coupled carbon-nitrogen cycle, thus the model may overestimate CO₂ fertilization
681 effects. On the contrary, implementation of drought-dependent phenology may amplify
682 drought inhibition effects on photosynthesis and result in an underestimation of carbon
683 uptake.

684

685 We estimated global trends of BVOC emissions with two schemes. Simulations with
686 PS_BVOC scheme show increasing isoprene emissions, mainly attributed to the increases
687 of temperature. For this scheme, CO₂ effects are neutralized due to both fertilization (on
688 photosynthesis) and inhibition (on isoprene). Simulations with MEGAN scheme show
689 decreasing emissions of isoprene and monoterpene because of CO₂ inhibition, especially
690 in the tropics. In subtropical areas, both schemes predict regional increases of BVOC

691 emissions in Europe following the warming trend and afforestation, but reductions in the
692 U.S. and China due to cropland expansion.

693

694

695 *Acknowledgements.* Funding support for this research is provided by the NASA
696 Atmospheric Composition Campaign Data Analysis and Modeling Program. This project
697 was supported in part by the facilities and staff of the Yale University Faculty of Arts and
698 Sciences High Performance Computing Center.

699

700

701 **References**

- 702 Ainsworth, E. A., and Long, S. P.: What have we learned from 15 years of free-air CO₂
703 enrichment (FACE)? A meta-analytic review of the responses of photosynthesis,
704 canopy, *New Phytol*, 165, 351-371, doi:10.1111/J.1469-8137.2004.01224.X, 2005.
- 705 Arneth, A., Niinemets, U., Pressley, S., Back, J., Hari, P., Karl, T., Noe, S., Prentice, I.
706 C., Serca, D., Hickler, T., Wolf, A., and Smith, B.: Process-based estimates of
707 terrestrial ecosystem isoprene emissions: incorporating the effects of a direct CO₂-
708 isoprene interaction, *Atmos Chem Phys*, 7, 31-53, doi:10.5194/acp-7-31-2007, 2007.
- 709 Barlow, J. M., Palmer, P. I., Bruhwiler, L. M., and Tans, P.: Analysis of CO₂ mole
710 fraction data: first evidence of large-scale changes in CO₂ uptake at high northern
711 latitudes, *Atmos. Chem. Phys. Discuss.*, 15, 7089-7139, doi:10.5194/acpd-15-7089-
712 2015, 2015.
- 713 Beer, C., Reichstein, M., Tomelleri, E., Ciais, P., Jung, M., Carvalhais, N., Rodenbeck,
714 C., Arain, M. A., Baldocchi, D., Bonan, G. B., Bondeau, A., Cescatti, A., Lasslop, G.,
715 Lindroth, A., Lomas, M., Luysaert, S., Margolis, H., Oleson, K. W., Rouspard, O.,
716 Veenendaal, E., Viovy, N., Williams, C., Woodward, F. I., and Papale, D.: Terrestrial
717 Gross Carbon Dioxide Uptake: Global Distribution and Covariation with Climate,
718 *Science*, 329, 834-838, doi:10.1126/Science.1184984, 2010.
- 719 Buckley, P. T.: Isoprene emissions from a Florida scrub oak species grown in ambient
720 and elevated carbon dioxide, *Atmos Environ*, 35, 631-634, doi:10.1016/S1352-
721 2310(00)00332-0, 2001.
- 722 Buitenwerf, R., Rose, L., and Higgins, S. I.: Three decades of multi-dimensional change
723 in global leaf phenology, *Nat Clim Change*, 5, 364-368, 2015.
- 724 Carslaw, K. S., Boucher, O., Spracklen, D. V., Mann, G. W., Rae, J. G. L., Woodward,
725 S., and Kulmala, M.: A review of natural aerosol interactions and feedbacks within
726 the Earth system, *Atmos. Chem. Phys.*, 10, 1701-1737, doi:10.5194/acp-10-1701-
727 2010, 2010.
- 728 Centritto, M., Brilli, F., Fodale, R., and Loreto, F.: Different sensitivity of isoprene
729 emission, respiration and photosynthesis to high growth temperature coupled with
730 drought stress in black poplar (*Populus nigra*) saplings, *Tree Physiol*, 31, 275-286,
731 doi:10.1093/Treephys/Tpq112, 2011.
- 732 Ciais, P., Sabine, C., Bala, G., Bopp, L., Brovkin, V., Canadell, J., Chhabra, A., DeFries,
733 R., Galloway, J., Heimann, M., Jones, C., Le Quere, C., Myneni, R., Piao, S., and
734 Thornton, P.: Carbon and other biogeochemical cycles, in: *Climate Change 2013: The
735 Physical Science Basis. Contribution of Working Group I to the Fifth Assessment
736 Report of the Intergovernmental Panel on Climate Change*, edited by: Stocker, T. F.,
737 Qin, D., Plattner, G.-K., Tignor, M., Allen, S. K., Boschung, J., Nauels, A., Xia, Y.,
738 Bex, V., and Midgley, P. M., Cambridge University Press, Cambridge, United
739 Kingdom and New York, NY, USA, 465-570, 2013.
- 740 Collatz, G. J., Ball, J. T., Grivet, C., and Berry, J. A.: Physiological and Environmental-
741 Regulation of Stomatal Conductance, Photosynthesis and Transpiration - a Model
742 That Includes a Laminar Boundary-Layer, *Agr Forest Meteorol*, 54, 107-136,
743 doi:10.1016/0168-1923(91)90002-8, 1991.
- 744 Cox, P. M.: Description of the "TRIFFID" Dynamic Global Vegetation Model, Hadley
745 Centre technical note 24, Berks, UK, 2001.

746 Defries, R. S., Hansen, M. C., Townshend, J. R. G., Janetos, A. C., and Loveland, T. R.:
747 A new global 1-km dataset of percentage tree cover derived from remote sensing,
748 *Global Change Biol*, 6, 247-254, doi:10.1046/J.1365-2486.2000.00296.X, 2000.

749 Dragoni, D., Schmid, H. P., Wayson, C. A., Potter, H., Grimmond, C. S. B., and
750 Randolph, J. C.: Evidence of increased net ecosystem productivity associated with a
751 longer vegetated season in a deciduous forest in south-central Indiana, USA, *Global*
752 *Change Biol*, 17, 886-897, doi:10.1111/J.1365-2486.2010.02281.X, 2011.

753 Farquhar, G. D., Caemmerer, S. V., and Berry, J. A.: A Biochemical-Model of
754 Photosynthetic Co₂ Assimilation in Leaves of C-3 Species, *Planta*, 149, 78-90,
755 doi:10.1007/Bf00386231, 1980.

756 Guenther, A. B., Zimmerman, P. R., Harley, P. C., Monson, R. K., and Fall, R.: Isoprene
757 and Monoterpene Emission Rate Variability - Model Evaluations and Sensitivity
758 Analyses, *J. Geophys. Res.*, 98, 12609-12617, doi:10.1029/93jd00527, 1993.

759 Guenther, A. B., Hewitt, C. N., Erickson, D., Fall, R., Geron, C., Graedel, T., Harley, P.,
760 Klinger, L., Lerdau, M., McKay, W. A., Pierce, T., Scholes, B., Steinbrecher, R.,
761 Tallamraju, R., Taylor, J., and Zimmerman, P.: A Global-Model of Natural Volatile
762 Organic-Compound Emissions, *J. Geophys. Res.*, 100, 8873-8892,
763 doi:10.1029/94jd02950, 1995.

764 Guenther, A. B., Jiang, X., Heald, C. L., Sakulyanontvittaya, T., Duhl, T., Emmons, L.
765 K., and Wang, X.: The Model of Emissions of Gases and Aerosols from Nature
766 version 2.1 (MEGAN2.1): an extended and updated framework for modeling biogenic
767 emissions, *Geosci Model Dev*, 5, 1471-1492, doi:10.5194/Gmd-5-1471-2012, 2012.

768 Hansen, M. C., DeFries, R. S., Townshend, J. R. G., Carroll, M., Dimiceli, C., and
769 Sohlberg, R. A.: Global Percent Tree Cover at a Spatial Resolution of 500 Meters:
770 First Results of the MODIS Vegetation Continuous Fields Algorithm, *Earth Interact*,
771 7, 1-15, doi:10.1175/1087-3562(2003)007<0001:GPTCAA>2.0.CO;2, 2003.

772 Heald, C. L., Wilkinson, M. J., Monson, R. K., Alo, C. A., Wang, G. L., and Guenther,
773 A.: Response of isoprene emission to ambient CO₂ changes and implications for
774 global budgets, *Global Change Biol*, 15, 1127-1140, doi:10.1111/J.1365-
775 2486.2008.01802.X, 2009.

776 Heinsch, F. A., Zhao, M. S., Running, S. W., Kimball, J. S., Nemani, R. R., Davis, K. J.,
777 Bolstad, P. V., Cook, B. D., Desai, A. R., Ricciuto, D. M., Law, B. E., Oechel, W. C.,
778 Kwon, H., Luo, H. Y., Wofsy, S. C., Dunn, A. L., Munger, J. W., Baldocchi, D. D.,
779 Xu, L. K., Hollinger, D. Y., Richardson, A. D., Stoy, P. C., Siqueira, M. B. S.,
780 Monson, R. K., Burns, S. P., and Flanagan, L. B.: Evaluation of remote sensing based
781 terrestrial productivity from MODIS using regional tower eddy flux network
782 observations, *Ieee T Geosci Remote*, 44, 1908-1925, doi:10.1109/Tgrs.2005.853936,
783 2006.

784 Houghton, R. A.: How well do we know the flux of CO₂ from land-use change?, *Tellus*
785 *B*, 62, 337-351, doi:Doi 10.1111/J.1600-0889.2010.00473.X, 2010.

786 Hurtt, G. C., Chini, L. P., Frolking, S., Betts, R. A., Feddema, J., Fischer, G., Fisk, J. P.,
787 Hibbard, K., Houghton, R. A., Janetos, A., Jones, C. D., Kindermann, G., Kinoshita,
788 T., Goldewijk, K. K., Riahi, K., Shevliakova, E., Smith, S., Stehfest, E., Thomson, A.,
789 Thornton, P., van Vuuren, D. P., and Wang, Y. P.: Harmonization of land-use
790 scenarios for the period 1500-2100: 600 years of global gridded annual land-use

791 transitions, wood harvest, and resulting secondary lands, *Climatic Change*, 109, 117-
792 161, doi:10.1007/S10584-011-0153-2, 2011.

793 Jeong, S. J., Ho, C. H., Gim, H. J., and Brown, M. E.: Phenology shifts at start vs. end of
794 growing season in temperate vegetation over the Northern Hemisphere for the period
795 1982-2008, *Global Change Biol*, 17, 2385-2399, doi:10.1111/J.1365-
796 2486.2011.02397.X, 2011.

797 Jung, M., Reichstein, M., and Bondeau, A.: Towards global empirical upscaling of
798 FLUXNET eddy covariance observations: validation of a model tree ensemble
799 approach using a biosphere model, *Biogeosciences*, 6, 2001-2013, doi:10.5194/bg-6-
800 2001-2009, 2009.

801 Keenan, T. F., Gray, J., Friedl, M. A., Toomey, M., Bohrer, G., Hollinger, D. Y.,
802 Munger, J. W., O'Keefe, J., Schmid, H. P., SueWing, I., Yang, B., and Richardson, A.
803 D.: Net carbon uptake has increased through warming-induced changes in temperate
804 forest phenology, *Nat Clim Change*, 4, 598-604, doi:10.1038/Nclimate2253, 2014.

805 Kivimaenpaa, M., Riikonen, J., Ahonen, V., Tervahauta, A., and Holopainen, T.:
806 Sensitivity of Norway spruce physiology and terpenoid emission dynamics to
807 elevated ozone and elevated temperature under open-field exposure, *Environ Exp*
808 *Bot*, 90, 32-42, doi:10.1016/J.Envexpbot.2012.1t004, 2013.

809 Lathiere, J., Hauglustaine, D. A., Friend, A. D., De Noblet-Ducoudre, N., Viovy, N., and
810 Folberth, G. A.: Impact of climate variability and land use changes on global biogenic
811 volatile organic compound emissions, *Atmos Chem Phys*, 6, 2129-2146,
812 doi:10.5194/acp-6-2129-2006, 2006.

813 Le Quere, C., Raupach, M. R., Canadell, J. G., Marland, G., Bopp, L., Ciais, P., Conway,
814 T. J., Doney, S. C., Feely, R. A., Foster, P., Friedlingstein, P., Gurney, K., Houghton,
815 R. A., House, J. I., Huntingford, C., Levy, P. E., Lomas, M. R., Majkut, J., Metzl, N.,
816 Ometto, J. P., Peters, G. P., Prentice, I. C., Randerson, J. T., Running, S. W.,
817 Sarmiento, J. L., Schuster, U., Sitch, S., Takahashi, T., Viovy, N., van der Werf, G.
818 R., and Woodward, F. I.: Trends in the sources and sinks of carbon dioxide, *Nat*
819 *Geosci*, 2, 831-836, doi:10.1038/Ngeo689, 2009.

820 Li, Z. R., Ratliff, E. A., and Sharkey, T. D.: Effect of Temperature on Postillumination
821 Isoprene Emission in Oak and Poplar, *Plant Physiol*, 155, 1037-1046,
822 doi:10.1104/Pp.110.167551, 2011.

823 Liang, J. Y., Xia, J. Y., Liu, L. L., and Wan, S. Q.: Global patterns of the responses of
824 leaf-level photosynthesis and respiration in terrestrial plants to experimental warming,
825 *J Plant Ecol*, 6, 437-447, doi:10.1093/Jpe/Rtt003, 2013.

826 Mao, J. F., Shi, X. Y., Thornton, P. E., Hoffman, F. M., Zhu, Z. C., and Myneni, R. B.:
827 Global Latitudinal-Asymmetric Vegetation Growth Trends and Their Driving
828 Mechanisms: 1982-2009, *Remote Sens*, 5, 1484-1497, doi:Doi 10.3390/Rs5031484,
829 2013.

830 Marais, E. A., Jacob, D. J., Kurosu, T. P., Chance, K., Murphy, J. G., Reeves, C., Mills,
831 G., Casadio, S., Millet, D. B., Barkley, M. P., Paulot, F., and Mao, J.: Isoprene
832 emissions in Africa inferred from OMI observations of formaldehyde columns,
833 *Atmos Chem Phys*, 12, 6219-6235, doi:10.5194/Acp-12-6219-2012, 2012.

834 Meinshausen, M., Smith, S. J., Calvin, K., Daniel, J. S., Kainuma, M. L. T., Lamarque, J.
835 F., Matsumoto, K., Montzka, S. A., Raper, S. C. B., Riahi, K., Thomson, A., Velders,
836 G. J. M., and van Vuuren, D. P. P.: The RCP greenhouse gas concentrations and their

837 extensions from 1765 to 2300, *Climatic Change*, 109, 213-241, doi:10.1007/S10584-
838 011-0156-Z, 2011.

839 Monson, R. K., Trahan, N., Rosenstiel, T. N., Veres, P., Moore, D., Wilkinson, M.,
840 Norby, R. J., Volder, A., Tjoelker, M. G., Briske, D. D., Karnosky, D. F., and Fall,
841 R.: Isoprene emission from terrestrial ecosystems in response to global change:
842 minding the gap between models and observations, *Philos T R Soc A*, 365, 1677-
843 1695, doi:10.1098/Rsta.2007.2038, 2007.

844 Muller, J. F., Stavrou, T., Wallens, S., De Smedt, I., Van Roozendael, M., Potosnak,
845 M. J., Rinne, J., Munger, B., Goldstein, A., and Guenther, A. B.: Global isoprene
846 emissions estimated using MEGAN, ECMWF analyses and a detailed canopy
847 environment model, *Atmos Chem Phys*, 8, 1329-1341, 2008.

848 Naik, V., Delire, C., and Wuebbles, D. J.: Sensitivity of global biogenic isoprenoid
849 emissions to climate variability and atmospheric CO₂, *J. Geophys. Res.*, 109,
850 D06301, doi:10.1029/2003jd004236, 2004.

851 Niinemets, U., Tenhunen, J. D., Harley, P. C., and Steinbrecher, R.: A model of isoprene
852 emission based on energetic requirements for isoprene synthesis and leaf
853 photosynthetic properties for Liquidambar and Quercus, *Plant Cell Environ*, 22,
854 1319-1335, doi:10.1046/j.1365-3040.1999.00505.x, 1999.

855 Niinemets, U., and Sun, Z. H.: How light, temperature, and measurement and growth
856 [CO₂] interactively control isoprene emission in hybrid aspen, *J Exp Bot*, 66, 841-
857 851, doi:10.1093/Jxb/Eru443, 2015.

858 Norby, R. J., DeLucia, E. H., Gielen, B., Calfapietra, C., Giardina, C. P., King, J. S.,
859 Ledford, J., McCarthy, H. R., Moore, D. J. P., Ceulemans, R., De Angelis, P., Finzi,
860 A. C., Karnosky, D. F., Kubiske, M. E., Lukac, M., Pregitzer, K. S., Scarascia-
861 Mugnozza, G. E., Schlesinger, W. H., and Oren, R.: Forest response to elevated CO₂
862 is conserved across a broad range of productivity, *P Natl Acad Sci USA*, 102, 18052-
863 18056, doi:10.1073/Pnas.0509478102, 2005.

864 Oleson, K. W., Lawrence, D. M., Bonan, G. B., Drewniak, B., Huang, M., Koven, C. D.,
865 Levis, S., Li, F., Riley, W. J., Subin, Z. M., Swenson, S. C., Thornton, P. E.,
866 Bozbiyik, A., Fisher, R., Heald, C. L., Kluzek, E., Lamarque, J.-F., Lawrence, P. J.,
867 Leung, L. R., Lipscomb, W., Muszala, S., Ricciuto, D. M., Sacks, W., Sun, Y., Tang,
868 J., and Yang, Z.-L.: Technical Description of version 4.5 of the Community Land
869 Model (CLM), National Center for Atmospheric Research, Boulder, CONCAR
870 Technical Note NCAR/TN-478+STR, 434, 2013.

871 Palmer, P. I., Abbot, D. S., Fu, T. M., Jacob, D. J., Chance, K., Kurosu, T. P., Guenther,
872 A., Wiedinmyer, C., Stanton, J. C., Pilling, M. J., Pressley, S. N., Lamb, B., and
873 Sumner, A. L.: Quantifying the seasonal and interannual variability of North
874 American isoprene emissions using satellite observations of the formaldehyde
875 column, *J Geophys Res-Atmos*, 111, D12315, doi:10.1029/2005jd006689, 2006.

876 Pan, Y. D., Birdsey, R. A., Fang, J. Y., Houghton, R., Kauppi, P. E., Kurz, W. A.,
877 Phillips, O. L., Shvidenko, A., Lewis, S. L., Canadell, J. G., Ciais, P., Jackson, R. B.,
878 Pacala, S. W., McGuire, A. D., Piao, S. L., Rautiainen, A., Sitch, S., and Hayes, D.: A
879 Large and Persistent Carbon Sink in the World's Forests, *Science*, 333, 988-993,
880 doi:10.1126/Science.1201609, 2011.

881 Pegoraro, E., Rey, A., Abrell, L., Vanharen, J., and Lin, G. H.: Drought effect on
882 isoprene production and consumption in Biosphere 2 tropical rainforest, *Global*
883 *Change Biol*, 12, 456-469, doi:Doi 10.1111/J.1365-2486.2006.01112.X, 2006.

884 Piao, S. L., Friedlingstein, P., Ciais, P., Viovy, N., and Demarty, J.: Growing season
885 extension and its impact on terrestrial carbon cycle in the Northern Hemisphere over
886 the past 2 decades, *Global Biogeochem Cy*, 21, Gb3018, doi:10.1029/2006gb002888,
887 2007.

888 Piao, S. L., Sitch, S., Ciais, P., Friedlingstein, P., Peylin, P., Wang, X. H., Ahlstrom, A.,
889 Anav, A., Canadell, J. G., Cong, N., Huntingford, C., Jung, M., Levis, S., Levy, P. E.,
890 Li, J. S., Lin, X., Lomas, M. R., Lu, M., Luo, Y. Q., Ma, Y. C., Myneni, R. B.,
891 Poulter, B., Sun, Z. Z., Wang, T., Viovy, N., Zaehle, S., and Zeng, N.: Evaluation of
892 terrestrial carbon cycle models for their response to climate variability and to CO₂
893 trends, *Global Change Biol*, 19, 2117-2132, doi:10.1111/Gcb.12187, 2013.

894 Possell, M., Hewitt, C. N., and Beerling, D. J.: The effects of glacial atmospheric CO₂
895 concentrations and climate on isoprene emissions by vascular plants, *Global Change*
896 *Biol*, 11, 60-69, doi:10.1111/J.1365-2486.2004.00889.X, 2005.

897 Ramankutty, N., and Foley, J. A.: Estimating historical changes in global land cover:
898 Croplands from 1700 to 1992, *Global Biogeochem Cy*, 13, 997-1027,
899 doi:10.1029/1999gb900046, 1999.

900 Richardson, A. D., Hollinger, D. Y., Dail, D. B., Lee, J. T., Munger, J. W., and O'Keefe,
901 J.: Influence of spring phenology on seasonal and annual carbon balance in two
902 contrasting New England forests, *Tree Physiol*, 29, 321-331, doi:Doi
903 10.1093/Treephys/Tpn040, 2009.

904 Richardson, A. D., Anderson, R. S., Arain, M. A., Barr, A. G., Bohrer, G., Chen, G. S.,
905 Chen, J. M., Ciais, P., Davis, K. J., Desai, A. R., Dietze, M. C., Dragoni, D., Garrity,
906 S. R., Gough, C. M., Grant, R., Hollinger, D. Y., Margolis, H. A., McCaughey, H.,
907 Migliavacca, M., Monson, R. K., Munger, J. W., Poulter, B., Raczka, B. M., Ricciuto,
908 D. M., Sahoo, A. K., Schaefer, K., Tian, H. Q., Vargas, R., Verbeeck, H., Xiao, J. F.,
909 and Xue, Y. K.: Terrestrial biosphere models need better representation of vegetation
910 phenology: results from the North American Carbon Program Site Synthesis, *Global*
911 *Change Biol*, 18, 566-584, doi:10.1111/J.1365-2486.2011.02562.X, 2012.

912 Richardson, A. D., Keenan, T. F., Migliavacca, M., Ryu, Y., Sonnentag, O., and Toomey,
913 M.: Climate change, phenology, and phenological control of vegetation feedbacks to
914 the climate system, *Agr Forest Meteorol*, 169, 156-173, 2013.

915 Ruehr, N. K., Martin, J. G., and Law, B. E.: Effects of water availability on carbon and
916 water exchange in a young ponderosa pine forest: Above- and belowground
917 responses, *Agr Forest Meteorol*, 164, 136-148, doi:10.1016/J.Agrformet.2012.05.015,
918 2012.

919 Sarmiento, J. L., Gloor, M., Gruber, N., Beaulieu, C., Jacobson, A. R., Fletcher, S. E. M.,
920 Pacala, S., and Rodgers, K.: Trends and regional distributions of land and ocean
921 carbon sinks, *Biogeosciences*, 7, 2351-2367, doi:10.5194/Bg-7-2351-2010, 2010.

922 Schaefer, K., Collatz, G. J., Tans, P., Denning, A. S., Baker, I., Berry, J., Prihodko, L.,
923 Suits, N., and Philpott, A.: Combined Simple Biosphere/Carnegie-Ames-Stanford
924 Approach terrestrial carbon cycle model, *J. Geophys. Res.*, 113, G03034,
925 doi:10.1029/2007jg000603, 2008.

926 Scott, C. E., Rap, A., Spracklen, D. V., Forster, P. M., Carslaw, K. S., Mann, G. W.,
927 Pringle, K. J., Kivekas, N., Kulmala, M., Lihavainen, H., and Tunved, P.: The direct
928 and indirect radiative effects of biogenic secondary organic aerosol, *Atmos Chem*
929 *Phys*, 14, 447-470, doi:10.5194/Acp-14-447-2014, 2014.

930 Sindelarova, K., Granier, C., Bouarar, I., Guenther, A., Tilmes, S., Stavrakou, T., Muller,
931 J. F., Kuhn, U., Stefani, P., and Knorr, W.: Global data set of biogenic VOC
932 emissions calculated by the MEGAN model over the last 30 years, *Atmos Chem*
933 *Phys*, 14, 9317-9341, doi:10.5194/Acp-14-9317-2014, 2014.

934 Sitch, S., Friedlingstein, P., Gruber, N., Jones, S. D., Murray-Tortarolo, G., Ahlström, A.,
935 Doney, S. C., Graven, H., Heinze, C., Huntingford, C., Levis, S., Levy, P. E., Lomas,
936 M., Poulter, B., Viovy, N., Zaehle, S., Zeng, N., Arneth, A., Bonan, G., Bopp, L.,
937 Canadell, J. G., Chevallier, F., Ciais, P., Ellis, R., Gloor, M., Peylin, P., Piao, S. L.,
938 Quéré, C. L., Smith, B., Zhu, Z., and Myneni, R.: Recent trends and drivers of
939 regional sources and sinks of carbon dioxide, *Biogeosciences*, 12, 653-679, 2015.

940 Stavrakou, T., Muller, J. F., Bauwens, M., De Smedt, I., Van Roozendaal, M., Guenther,
941 A., Wild, M., and Xia, X.: Isoprene emissions over Asia 1979-2012: impact of
942 climate and land-use changes, *Atmos Chem Phys*, 14, 4587-4605, doi:10.5194/Acp-
943 14-4587-2014, 2014.

944 Sun, Z. H., Hve, K., Vislap, V., and Niinemets, U.: Elevated [CO₂] magnifies isoprene
945 emissions under heat and improves thermal resistance in hybrid aspen, *J Exp Bot*, 64,
946 5509-5523, doi:10.1093/Jxb/Ert318, 2013.

947 Unger, N., Harper, K., Zheng, Y., Kiang, N. Y., Aleinov, I., Arneth, A., Schurgers, G.,
948 Amelynck, C., Goldstein, A., Guenther, A., Heinesch, B., Hewitt, C. N., Karl, T.,
949 Laffineur, Q., Langford, B., McKinney, K. A., Misztal, P., Potosnak, M., Rinne, J.,
950 Pressley, S., Schoon, N., and Serça, D.: Photosynthesis-dependent isoprene emission
951 from leaf to planet in a global carbon-chemistry-climate model, *Atmos. Chem. Phys.*,
952 13, 10243-10269, doi:10.5194/acp-13-10243-2013, 2013.

953 Unger, N.: On the role of plant volatiles in anthropogenic global climate change,
954 *Geophys Res Lett*, 41, 8563-8569, doi:10.1002/2014gl061616, 2014.

955 Uppala, S. M., Kallberg, P. W., Simmons, A. J., Andrae, U., Bechtold, V. D., Fiorino,
956 M., Gibson, J. K., Haseler, J., Hernandez, A., Kelly, G. A., Li, X., Onogi, K.,
957 Saarinen, S., Sokka, N., Allan, R. P., Andersson, E., Arpe, K., Balmaseda, M. A.,
958 Beljaars, A. C. M., Van De Berg, L., Bidlot, J., Bormann, N., Caires, S., Chevallier,
959 F., Dethof, A., Dragosavac, M., Fisher, M., Fuentes, M., Hagemann, S., Holm, E.,
960 Hoskins, B. J., Isaksen, L., Janssen, P. A. E. M., Jenne, R., McNally, A. P., Mahfouf,
961 J. F., Morcrette, J. J., Rayner, N. A., Saunders, R. W., Simon, P., Sterl, A., Trenberth,
962 K. E., Untch, A., Vasiljevic, D., Viterbo, P., and Woollen, J.: The ERA-40 re-
963 analysis, *Q J Roy Meteor Soc*, 131, 2961-3012, doi:10.1256/Qj.04.176, 2005.

964 von Caemmerer, S., and Farquhar, G. D.: Some Relationships between the Biochemistry
965 of Photosynthesis and the Gas-Exchange of Leaves, *Planta*, 153, 376-387, 1981.

966 Weedon, G. P., Gomes, S., Viterbo, P., Shuttleworth, W. J., Blyth, E., Osterle, H., Adam,
967 J. C., Bellouin, N., Boucher, O., and Best, M.: Creation of the WATCH Forcing Data
968 and Its Use to Assess Global and Regional Reference Crop Evaporation over Land
969 during the Twentieth Century, *J Hydrometeorol*, 12, 823-848,
970 doi:10.1175/2011jhm1369.1, 2011.

971 Weedon, G. P., Balsamo, G., Bellouin, N., Gomes, S., Best, M. J., and Viterbo, P.: The
972 WFDEI meteorological forcing data set: WATCH Forcing Data methodology applied
973 to ERA-Interim reanalysis data, *Water Resources Research*, 50, 7505-7514,
974 doi:10.1002/2014wr015638, 2014.

975 Wofsy, S. C., Goulden, M. L., Munger, J. W., Fan, S. M., Bakwin, P. S., Daube, B. C.,
976 Bassow, S. L., and Bazzaz, F. A.: Net Exchange of Co₂ in a Midlatitude Forest,
977 *Science*, 260, 1314-1317, doi:10.1126/Science.260.5112.1314, 1993.

978 Wu, Z. T., Dijkstra, P., Koch, G. W., Penuelas, J., and Hungate, B. A.: Responses of
979 terrestrial ecosystems to temperature and precipitation change: a meta-analysis of
980 experimental manipulation, *Global Change Biol*, 17, 927-942, doi:10.1111/J.1365-
981 2486.2010.02302.X, 2011.

982 Xia, J. B., Zhang, G. C., Wang, R. R., and Zhang, S. Y.: Effect of soil water availability
983 on photosynthesis in *Ziziphus jujuba* var. *spinosa* in a sand habitat formed from
984 seashells: Comparison of four models, *Photosynthetica*, 52, 253-261, doi:Doi
985 10.1007/S11099-014-0030-0, 2014.

986 Yue, X., and Unger, N.: Ozone vegetation damage effects on gross primary productivity
987 in the United States, *Atmos. Chem. Phys.*, 14, 9137-9153, doi:10.5194/acp-14-9137-
988 2014, 2014.

989 Yue, X., and Unger, N.: The Yale Interactive terrestrial Biosphere model: description,
990 evaluation and implementation into NASA GISS ModelE2, *Geosci. Model Dev.*, 8,
991 2399-2417, doi:10.5194/gmd-8-2399-2015, 2015.

992 Yue, X., Unger, N., Keenan, T. F., Zhang, X., and Vogel, C. S.: Probing the past 30-year
993 phenology trend of U.S. deciduous forests, *Biogeosciences*, 12, 4693-4709,
994 doi:10.5194/bg-12-4693-2015, 2015.

995 Zhao, M. S., Heinsch, F. A., Nemani, R. R., and Running, S. W.: Improvements of the
996 MODIS terrestrial gross and net primary production global data set, *Remote Sens
997 Environ*, 95, 164-176, doi:10.1016/J.Rse.2004.12.011, 2005.

998 Zhao, M. S., and Running, S. W.: Drought-Induced Reduction in Global Terrestrial Net
999 Primary Production from 2000 Through 2009, *Science*, 329, 940-943,
1000 doi:10.1126/Science.1192666, 2010.

1001 Zheng, Y., Unger, N., Barley, M., and Yue, X.: Relationships between photosynthesis
1002 and formaldehyde as a probe of isoprene emission, *Atmos. Chem. Phys.*, 15, 8559-
1003 8576, doi:10.5194/acp-15-8559-2015, 2015.

1004 Zhu, Z. C., Bi, J., Pan, Y. Z., Ganguly, S., Anav, A., Xu, L., Samanta, A., Piao, S. L.,
1005 Nemani, R. R., and Myneni, R. B.: Global Data Sets of Vegetation Leaf Area Index
1006 (LAI)3g and Fraction of Photosynthetically Active Radiation (FPAR)3g Derived
1007 from Global Inventory Modeling and Mapping Studies (GIMMS) Normalized
1008 Difference Vegetation Index (NDVI3g) for the Period 1981 to 2011, *Remote Sens*, 5,
1009 927-948, doi:10.3390/Rs5020927, 2013.

1010

1011

1012
1013
1014
1015

Table 1. Summary of model simulations driven with WFDEI reanalysis.

Simulations	Descriptions
CO2_MET_LUC	Annually updated [CO ₂] and land cover, and hourly meteorology. All forcings vary for 1980-2011.
CO2_MET	Annually updated [CO ₂] and hourly meteorology for 1980-2011, land cover is prescribed at the year 1980.
CO2_ONLY	Annually updated [CO ₂] for 1980-2011, land cover is prescribed and hourly meteorology is recycled for the year 1980.
MET_ONLY	Hourly meteorology varies for 1980-2011. [CO ₂] and land cover are prescribed at the year 1980.
LUC_ONLY	Annually updated land cover for 1980-2011, [CO ₂] is prescribed and hourly meteorology is recycled for the year 1980.
TEMP_ONLY	Hourly temperature for 1980-2011 but other meteorological variables are recycled for 1980. [CO ₂] and land cover are prescribed at the year 1980.
PAR_ONLY	Hourly PAR for 1980-2011 but other meteorological variables are recycled for 1980. [CO ₂] and land cover are prescribed at the year 1980.
SOILW_ONLY	Hourly soil wetness for 1980-2011 but other meteorological variables are recycled for 1980. [CO ₂] and land cover are prescribed at the year 1980.
LAI_ONLY	Hourly meteorology is recycled for the year 1980. [CO ₂] and land cover are prescribed at the year 1980. Leaf area index varies for 1980-2011.
PHEN_ONLY	Hourly meteorology is recycled for the year 1980. [CO ₂] and land cover are prescribed at the year 1980. Phenology varies for 1980-2011.

1016
1017
1018
1019
1020
1021

1022
 1023
 1024
 1025
 1026
 1027
 1028

Table 2. Summary of trends in different domains from the simulation CO2_MET_LUC, which is driven with WFDEI meteorology. Significant trends ($p < 0.05$) are indicated with asterisks.

Regions	Amazon	North America	Central Africa	Europe	East Asia	Indonesia
LAI ($10^{-3} \text{ m}^2 \text{ m}^{-2} \text{ a}^{-1}$)	0.8	0.4 *	1.8 *	3.5 *	-0.4 *	-0.1
GPP (Tg C a^{-2})	52.7 *	13.6	83.3 *	53.4 *	42.4 *	15.3 *
NPP (Tg C a^{-2})	27.1 *	9.7	51.7 *	33.2 *	27.2 *	11.4 *
NEP (Tg C a^{-2})	-8.1	-1.7	11.6	6.7	-6.2	0.2
Ra (Tg C a^{-2})	25.6 *	3.9	31.6 *	20.2 *	15.2 *	3.9 *
Rh (Tg C a^{-2})	35.2 *	11.2 *	39.8 *	26.6 *	33.4 *	11.2 *
Isoprene PS_BVOC (Tg C a^{-2})	0.04	-0.03	0.25 *	0.16 *	-0.02	-0.01
Isoprene MEGAN (Tg C a^{-2})	-0.43 *	-0.07 *	-0.14 *	0.10 *	-0.13 *	-0.16 *
Monoterpene (Tg C a^{-2})	-0.03 *	0.01	-0.002	0.03 *	-0.02 *	-0.02 *
Budburst (days a^{-1})	N/A ^a	-0.01	N/A	-0.16 *	-0.15 *	N/A
Dormancy onset (days a^{-1})	N/A	0.09 *	N/A	0.16 *	0.03	N/A
Season extension (days a^{-1})	N/A	0.1 *	N/A	0.32 *	0.18 *	N/A

1029
 1030
 1031

^a Phenology is set to constant for tropical rainforest in the model.

1032
 1033
 1034
 1035
 1036
 1037
 1038

Table 3. Summary of simulated trends of global carbon fluxes (Tg C a⁻²) from different experiments. Simulations are using WFDEI meteorology. Significant trends ($p < 0.05$) are indicated with asterisks.

Simulations	GPP	NPP	NEP	Ra	Rh
CO2_MET_LUC	297.4 *	185.3 *	2.7	112.1 *	180.9 *
CO2_MET	329.5 *	206.2 *	4.5	123.3 *	199.8 *
CO2_ONLY	412.4 *	299 *	66.2 *	113.5 *	231.9 *
MET_ONLY	-108.6 *	-108.2 *	-72.6 *	-0.4	-35
LUC_ONLY	-13 *	-8 *	-34.6 *	-5 *	26.9 *
TEMP_ONLY	-23.2 *	-56 *	-10.2 *	32.8 *	-43.6 *
PAR_ONLY	-5.9	-5.8	-23.4 *	-0.1	18.3 *
SOILW_ONLY	-84.8 *	-51 *	-13.1 *	-33.8 *	-38.3
LAI_ONLY	-8.8	-25.6 *	-44.5 *	16.7 *	18.7 *
PHEN_ONLY	-103.1 *	-56.2 *	47.1 *	-46.8 *	-102.9 *

1039
 1040

1041 **Figure Captions**

1042

1043 **Figure 1.** Comparison of trends in (b-f) simulated leaf area index (LAI) with (a)
1044 observations for 1982-2011. Observations are derived from GIMMS NDVI. Simulations
1045 are performed with either (d, e, f) single forcings or (b, c) the combinations of these
1046 forcings. Forcings considered include meteorology from WFDEI reanalysis (MET), CO₂
1047 fertilization (CO₂), and land use change (LUC). For every forcing included in the
1048 simulation, the year-to-year fields are utilized. Otherwise, the forcing is prescribed at the
1049 year 1980. Only significant trends ($p < 0.05$) are presented. The six box regions in (a)
1050 indicate areas for statistical analyses in Table 2.

1051

1052 **Figure 2.** Simulated trends in (a) gross primary productivity (GPP), (c) net primary
1053 productivity (NPP), and (e) net ecosystem productivity (NEP), and (b, d, f) the dominant
1054 drivers for these changes during 1982-2011. Simulations are performed with WFDEI
1055 reanalysis. Three factors, meteorological forcing, CO₂ fertilization, and land use change,
1056 are considered as the potential drivers of flux trends. For each grid in figures (b, d, f), the
1057 factor generating the largest (either maximum or minimum) trend with the same sign as
1058 the net change (a, c, e) is selected as the driving factor. Only significant trends ($p < 0.05$)
1059 are presented.

1060

1061 **Figure 3.** Comparisons of trends in (a, b) GPP and (c, d) NPP for 2000-2011 between (a,
1062 c) simulations and (b, d) observations. Observed fluxes are retrieved from the Moderate
1063 Resolution Imaging Spectroradiometer (MODIS).

1064

1065 **Figure 4.** Simulated (a) trends in GPP driven alone with WFDEI reanalysis and the (b)
1066 drivers for such changes. Simulation in (a) is performed with year-to-year meteorological
1067 forcings but prescribed [CO₂] and land use in the year 1980. Simulations in (b) are the
1068 same as (a) except that the year-to-year variations are allowed only for a single
1069 meteorological variable (temperature, PAR, or soil wetness) each time. For each grid, the
1070 meteorological variable generating the largest (either maximum or minimum) trend with

1071 the same sign as the net change (a) is selected as the driving factor. Only significant
1072 trends ($p < 0.05$) are presented.

1073

1074 **Figure 5.** Global total fluxes of GPP, NPP, Rh (heterotrophic respiration), and NEP from
1075 different sensitivity simulations with all forcings (black), meteorology alone (red), CO₂
1076 alone (green), and land use change alone (blue).

1077

1078 **Figure 6.** Simulated trends of (a, c) isoprene and (e) monoterpene, and (b, d, f) the
1079 dominant drivers for these changes during 1982-2011. Simulations are performed with
1080 WFDEI reanalysis. Isoprene emissions are simulated with (a) PS_BVOC and (c)
1081 MEGAN schemes. Three factors, meteorological forcing, CO₂ effects (both fertilization
1082 and inhibition), and land use change, are considered as the potential drivers of flux
1083 trends. For each grid in figures (b, d, f), the factor generating the largest (either maximum
1084 or minimum) trend with the same sign as the net change (a-c) is selected as the driving
1085 factor. Only significant trends ($p < 0.05$) are presented.

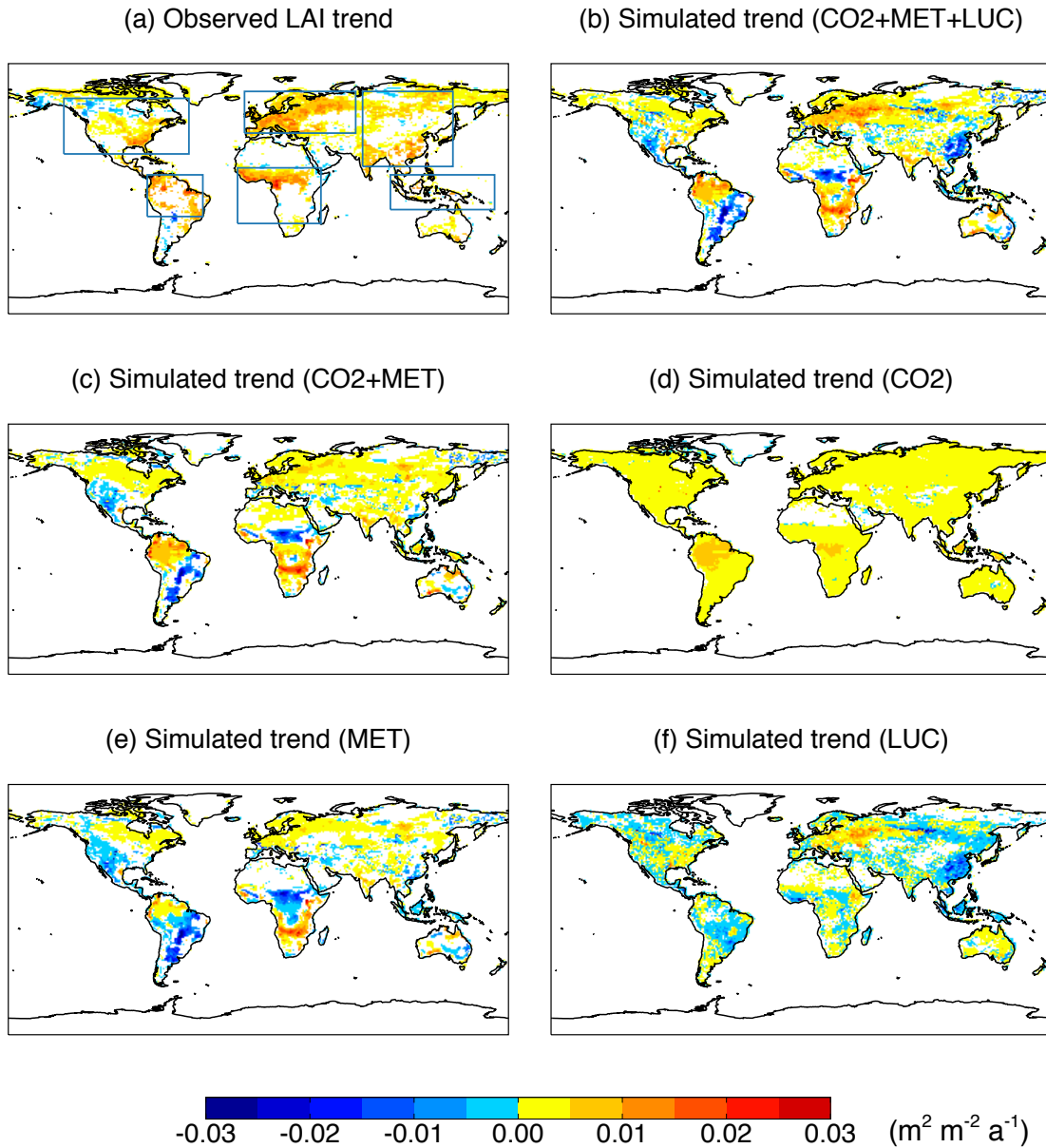
1086

1087 **Figure 7.** Responses of (a) GPP and (b) isoprene emissions to the changes in the annual
1088 average LAI at the north of 30°N for simulations CO₂_MET (red) and LAI_ONLY
1089 (blue). Both GPP and isoprene emissions are the sum of all PFTs. Isoprene is simulated
1090 with the PS_BVOC scheme. Units of trends are (a) Pg C a⁻¹ LAI⁻¹ and (b) Tg C a⁻¹ LAI⁻¹.
1091 The spatial distribution of GPP and isoprene changes is shown in Figure S2.

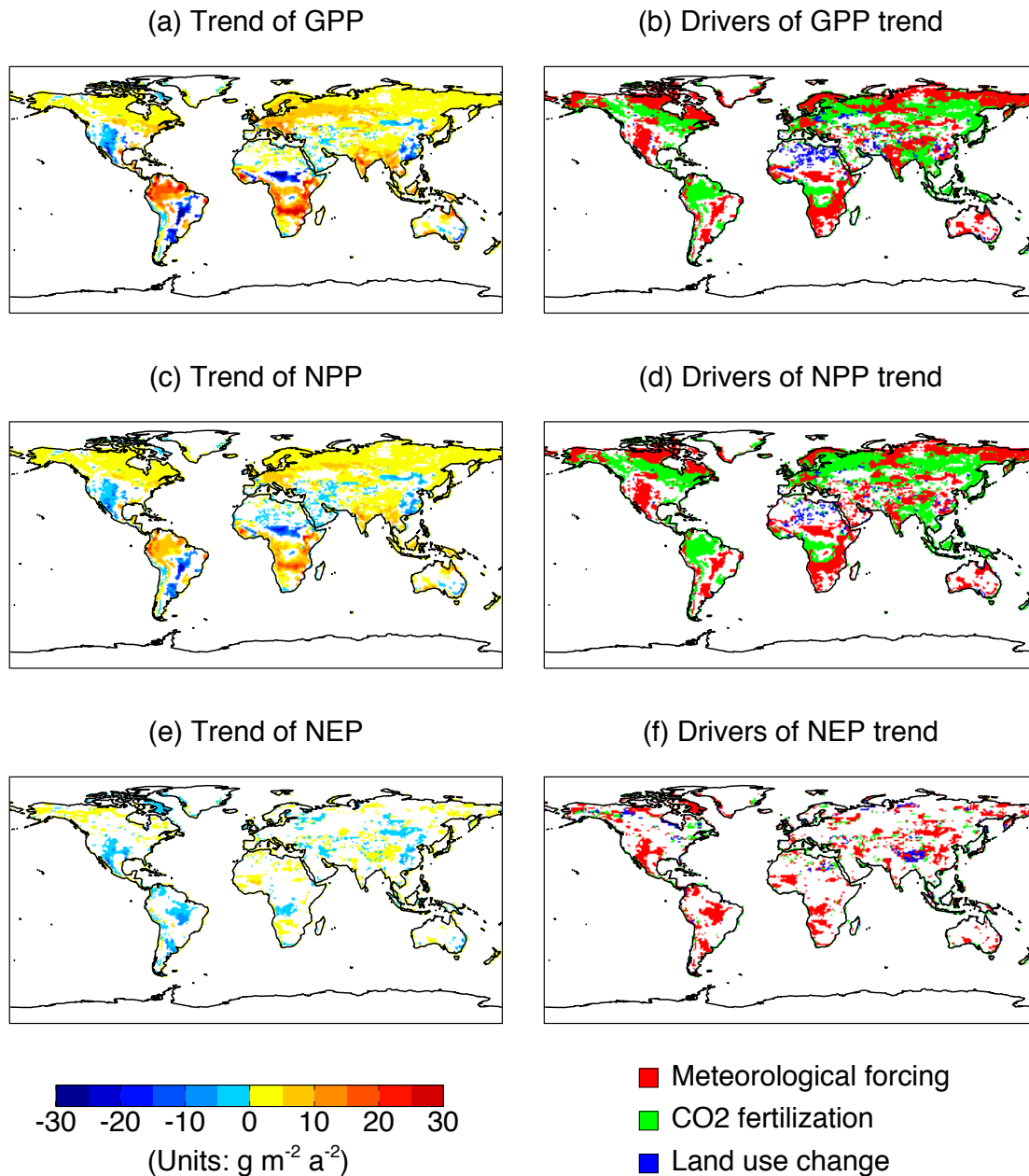
1092

1093 **Figure 8.** Predicted trend in (a) budburst and (b) dormancy onset dates over north of
1094 30°N and the responses of (c) GPP and (d) isoprene emissions to the changes in the
1095 growing length. Both GPP and isoprene emissions are the sum of DBF, shrub, grassland,
1096 and tundra. Isoprene is simulated with the PS_BVOC scheme. For the bottom panel,
1097 different colors indicate sensitivity experiments with different year-to-year forcings: CO₂
1098 and meteorology (red), temperature only (magenta), and phenology only (blue). Units of
1099 trends are (a) day a⁻¹, (b) day a⁻¹, (c) Pg C a⁻¹ day⁻¹, and (d) Tg C a⁻¹ day⁻¹. The spatial
1100 distribution of GPP and isoprene changes is shown in Figure S2.

1101



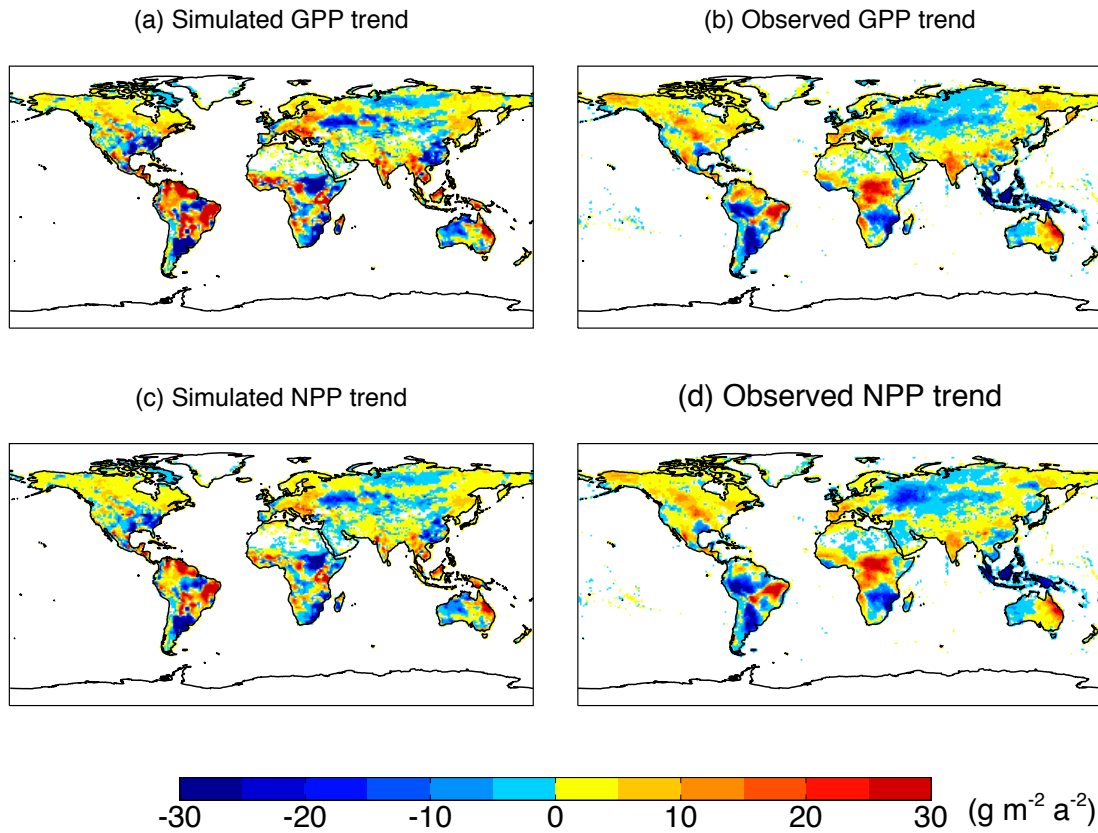
1102
 1103 **Figure 1.** Comparison of trends in (b-f) simulated leaf area index (LAI) with (a)
 1104 observations for 1982-2011. Observations are derived from GIMMS NDVI. Simulations
 1105 are performed with either (d, e, f) single forcings or (b, c) the combinations of these
 1106 forcings. Forcings considered include meteorology from WFDEI reanalysis (MET), CO₂
 1107 fertilization (CO₂), and land use change (LUC). For every forcing included in the
 1108 simulation, the year-to-year fields are utilized. Otherwise, the forcing is prescribed at the
 1109 year 1980. Only significant trends ($p < 0.05$) are presented. The six box regions in (a)
 1110 indicate areas for statistical analyses in Table 2.
 1111
 1112
 1113



1114
 1115 **Figure 2.** Simulated trends in (a) gross primary productivity (GPP), (c) net primary
 1116 productivity (NPP), and (e) net ecosystem productivity (NEP), and (b, d, f) the dominant
 1117 drivers for these changes during 1982-2011. Simulations are performed with WFDEI
 1118 reanalysis. Three factors, meteorological forcing, CO₂ fertilization, and land use change,
 1119 are considered as the potential drivers of flux trends. For each grid in figures (b, d, f), the
 1120 factor generating the largest (either maximum or minimum) trend with the same sign as
 1121 the net change (a, c, e) is selected as the driving factor. Only significant trends ($p < 0.05$)
 1122 are presented.

1123
 1124

1125
1126



1127
1128 **Figure 3.** Comparisons of trends in (a, b) GPP and (c, d) NPP for 2000-2011 between (a,
1129 c) simulations and (b, d) observations. Observed fluxes are retrieved from the Moderate
1130 Resolution Imaging Spectroradiometer (MODIS).

1131
1132
1133
1134
1135
1136
1137

1138
1139
1140
1141
1142
1143
1144
1145
1146
1147
1148
1149
1150
1151
1152
1153
1154
1155
1156
1157
1158
1159
1160
1161
1162
1163
1164
1165
1166
1167
1168
1169
1170
1171
1172
1173
1174
1175
1176

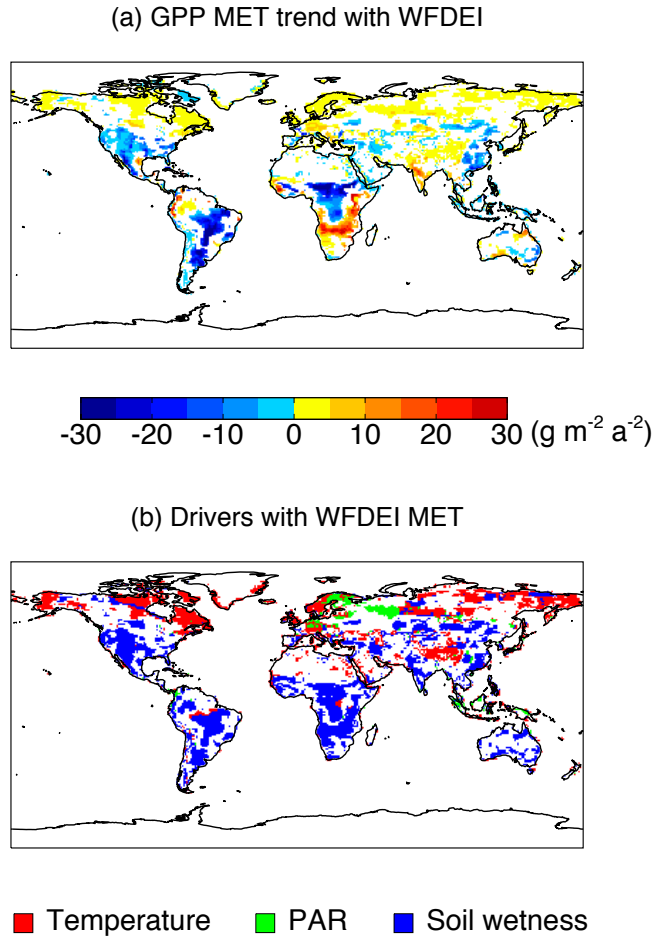
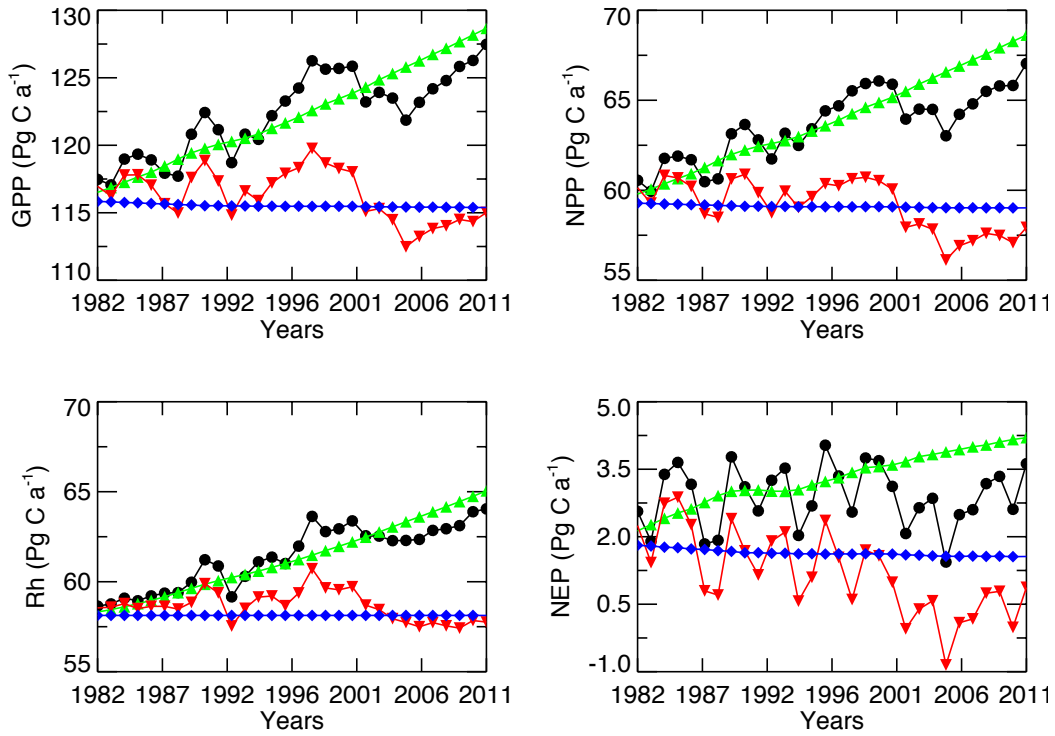
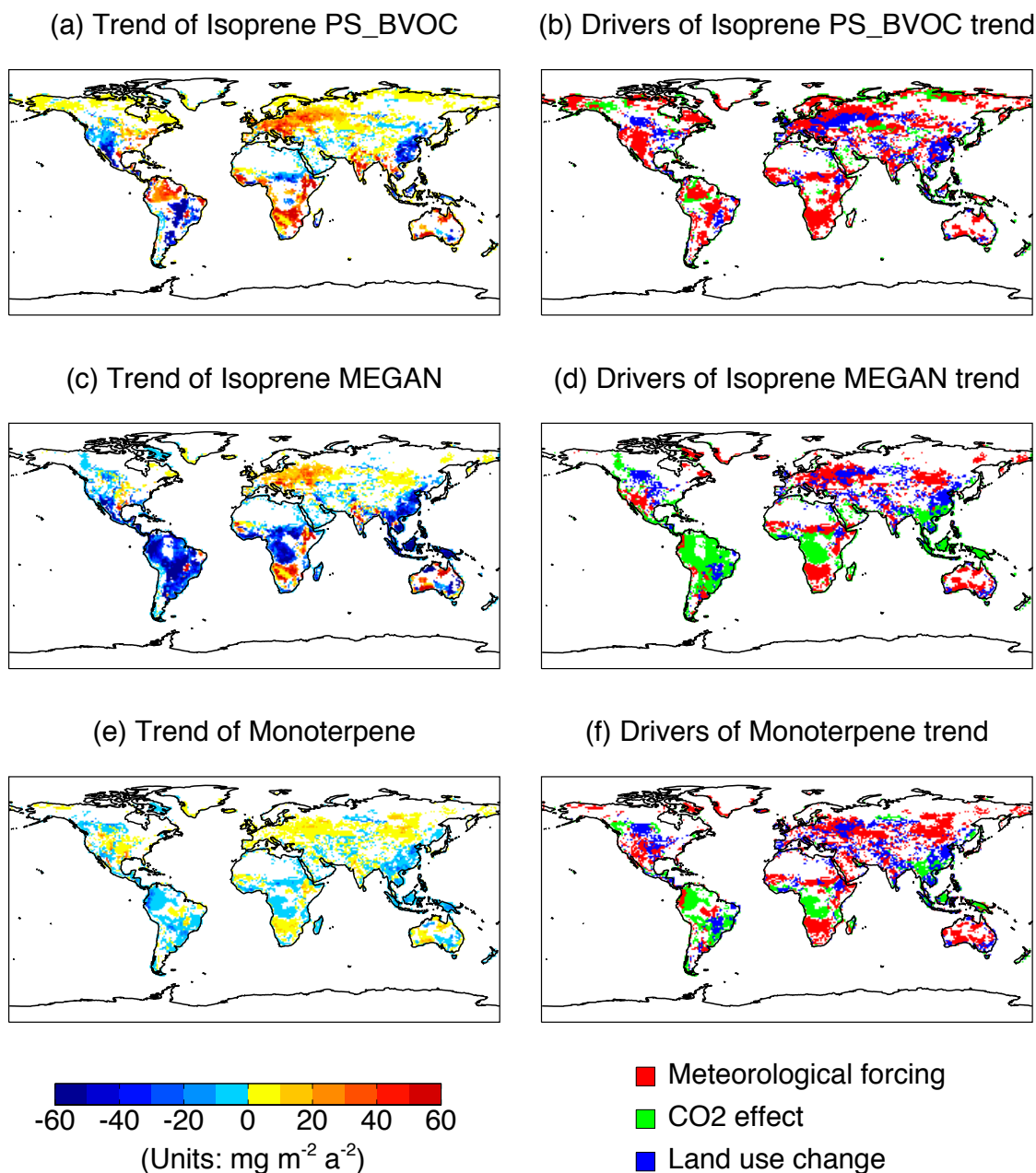


Figure 4. Simulated (a) trends in GPP driven alone with WFDEI reanalysis and the (b) drivers for such changes. Simulation in (a) is performed with year-to-year meteorological forcings but prescribed $[\text{CO}_2]$ and land use in the year 1980. Simulations in (b) are the same as (a) except that the year-to-year variations are allowed only for a single meteorological variable (temperature, PAR, or soil wetness) each time. For each grid, the meteorological variable generating the largest (either maximum or minimum) trend with the same sign as the net change (a) is selected as the driving factor. Only significant trends ($p < 0.05$) are presented.

1177
1178
1179
1180
1181
1182

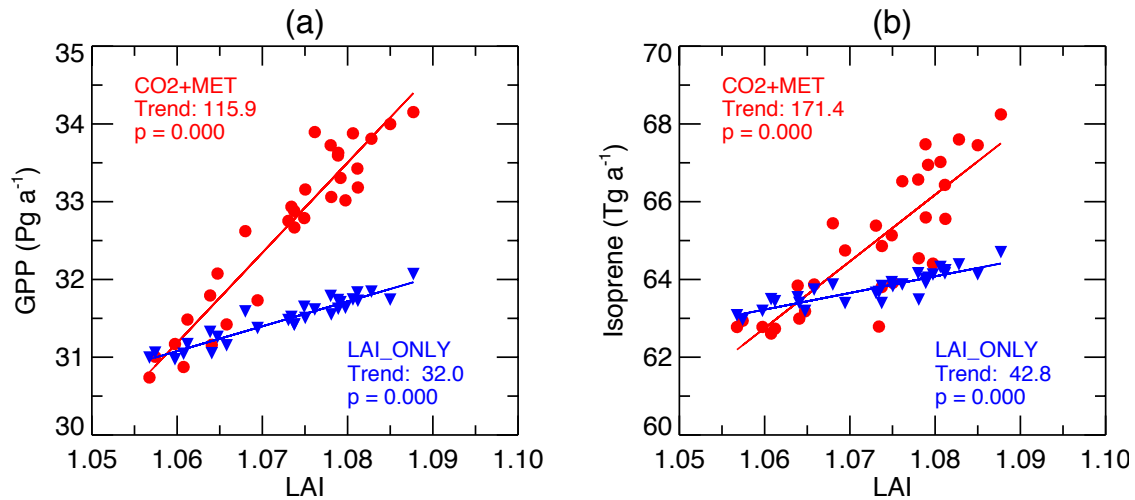


1183 **Figure 5.** Global total fluxes of GPP, NPP, Rh (heterotrophic respiration), and NEP from
1184 different sensitivity simulations with all forcings (black), meteorology only (red), CO₂
1185 alone (green), and land use change alone (blue).
1186



1187
 1188 **Figure 6.** Simulated trends of (a, c) isoprene and (e) monoterpene, and (b, d, f) the
 1189 dominant drivers for these changes during 1982-2011. Simulations are performed with
 1190 WFDEI reanalysis. Isoprene emissions are simulated with (a) PS_BVOC and (c)
 1191 MEGAN schemes. Three factors, meteorological forcing, CO₂ effects (both fertilization
 1192 and inhibition), and land use change, are considered as the potential drivers of flux
 1193 trends. For each grid in figures (b, d, f), the factor generating the largest (either maximum
 1194 or minimum) trend with the same sign as the net change (a-c) is selected as the driving
 1195 factor. Only significant trends ($p < 0.05$) are presented.
 1196

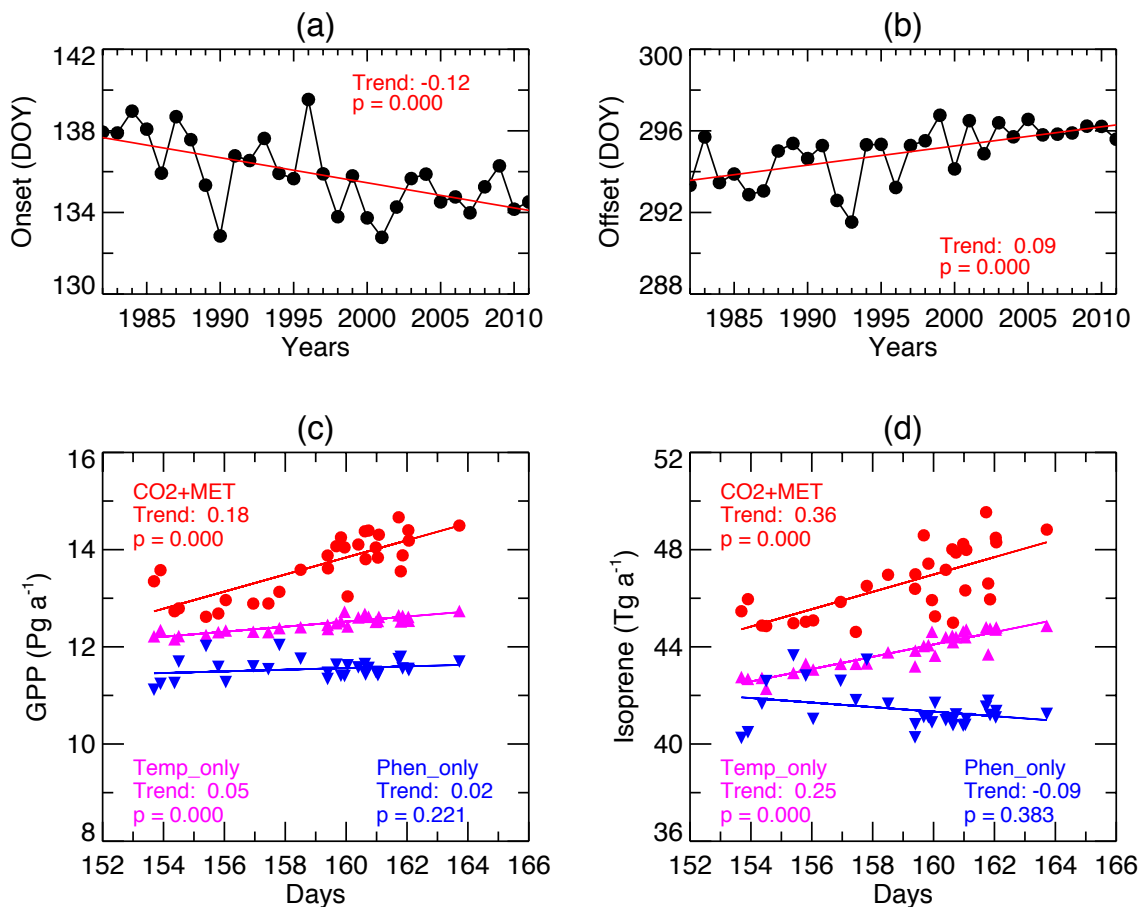
1197
1198
1199
1200
1201



1202
1203
1204
1205
1206
1207
1208
1209

Figure 7. Responses of (a) GPP and (b) isoprene emissions to the changes in the annual average LAI at the north of 30°N for simulations CO2_MET (red) and LAI_ONLY (blue). Both GPP and isoprene emissions are the sum of all PFTs. Isoprene is simulated with the PS_BVOC scheme. Units of trends are (a) Pg C a⁻¹ LAI⁻¹ and (b) Tg C a⁻¹ LAI⁻¹. The spatial distribution of GPP and isoprene changes is shown in Figure S2.

1210
1211



1212

1213 **Figure 8.** Predicted trend in (a) budburst and (b) dormancy onset dates over north of
1214 30°N and the responses of (c) GPP and (d) isoprene emissions to the changes in the
1215 growing length. Both GPP and isoprene emissions are the sum of DBF, shrub, grassland,
1216 and tundra. Isoprene is simulated with the PS_BVOC scheme. For the bottom panel,
1217 different colors indicate sensitivity experiments with different year-to-year forcings: CO₂
1218 and meteorology (red), temperature only (magenta), and phenology only (blue). Units of
1219 trends are (a) day a⁻¹, (b) day a⁻¹, (c) Pg C a⁻¹ day⁻¹, and (d) Tg C a⁻¹ day⁻¹. The spatial
1220 distribution of GPP and isoprene changes is shown in Figure S2.

1221

1222

1223